In Situ EQCM-D Investigations of PEMFC Catalyst-Ionomer Interactions

ChemElectroChem

Chemistry Europe
European Chemical Societies Publishing
ChemElectroChem

RESEARCH ARTICLE OPEN ACCESS

In Situ EQCM-D Investigations of PEMFC Catalyst-Ionomer Interactions

Nils Rieger[1] | Isak Almyren[1] | Linnéa Strandberg[1] | Martina Butori[2] | Rakel W. Lindström[2] | Björn Eriksson[2] | Patric Jannasch[3] | Björn Wickman[1]

[1]Department of Physics and Competence Center for Catalysis, Chalmers University of Technology, Göteborg, Sweden | [2]Department of Chemical Engineering, Applied Electrochemistry, KTH Royal Institute of Technology, Stockholm, Sweden | [3]Centre for Analysis and Synthesis, Lund University, Lund, Sweden

Correspondence: Nils Rieger (nils.rieger@chalmers.se) | Björn Wickman (bjorn.wickman@chalmers.se)

Received: 23 October 2025 | **Revised:** 15 December 2025 | **Accepted:** 8 January 2026

Keywords: catalyst–ionomer interaction | electrochemical quartz crystal microbalance | platinum | proton exchange membrane fuel cells | redox chemistry

ABSTRACT

Proton exchange membrane fuel cell (PEMFC) electrodes comprise multiple functional components whose interplay critically influences both performance and long-term stability. In this article, the interaction between ionomer and catalyst materials was investigated using electrochemical quartz crystal microbalance with dissipation monitoring, enabling detection of potential-dependent changes in mass and viscoelastic properties. Measurements were conducted on platinum, carbon, and gold electrodes, with and without a Nafion overlayer, in 0.5 M H_2SO_4 and 0.1 M $HClO_4$. Additionally, a representative catalyst layer (CL) was fabricated by spray-coating PEMFC catalyst ink onto quartz crystals and examined under identical electrochemical conditions. Enhanced hydration of Nafion on a platinum electrode was observed during potential cycling, attributed to electrochemical reactions at the platinum surface, rather than being a direct consequence of the applied potential as this behavior was not observed on crystals with Nafion-covered carbon electrodes. Changes in viscoelastic properties and mass uptake was shown to be influenced by the choice of electrolyte solution, particularly the nature of the anions. Importantly, the response of the spray-coated PEMFC-CL aligns closely with the behavior observed for Nafion-coated planar platinum, validating the simplified model approach and providing deeper insight into ionomer behavior under dynamic fuel cell conditions.

1 | Introduction

To mitigate the consequences of anthropogenic climate change, society must transition from fossil fuels to renewable energy sources, thereby significantly reducing greenhouse gas emissions. However, such a societal shift necessitates the development of advanced energy storage solutions, including the establishment of a robust hydrogen economy [1, 2]. This encompasses the development of efficient technologies for energy recovery from produced hydrogen, for which the proton exchange membrane fuel cell (PEMFC) is one such technology.

The performance of a PEMFC is strongly influenced by its constituent materials and the interactions between them. Particularly, the choice of catalyst is decisive for the performance of the fuel cell [3, 4]. In commercial applications, platinum nanoparticles (NPs) are commonly employed, with electrical contact facilitated by a porous carbon support. Similarly, the electrolyte material of the proton exchange membrane (PEM) as well as the ionomer material, predominantly composed of perfluorosulfonic acid (PFSA) polymers, play a critical role in the fuel cell efficiency [5]. The ionomer, together with the PEM, enables proton conduction, while maintaining hydration in the catalyst layer (CL) and still allowing gas access to active sites. Achieving an optimized balance between the key functions of the ionomer remains one of the central challenges in the continued development of PEMFCs, as these functions are inherently interdependent and

can influence each other in complex ways. For instance, the ionomer must facilitate efficient gas transport to the active sites, particularly at the cathode, which requires high O_2 permeability. Simultaneously, the polymer structure must support effective proton conduction to sustain electrochemical activity. Moreover, an excessive ionomer-to-catalyst or ionomer-to-carbon (I/C) ratio can negatively impact overall performance by hindering the gas diffusion and blocking or poisoning active sites [6–8]. In this context, a detailed mechanistic understanding of ionomer–catalyst interactions and the processes occurring at their interface is essential. Such insight is critical for designing CLs that strike the right balance between these competing requirements and thereby maximize the fuel cell efficiency.

Over the past decades, the influence of individual PEMFC electrode components on the overall performance has been extensively studied. The insights gained have enabled identification of several key contributors to performance limitations at the beginning of life, paving the way for development of targeted optimization strategies. One notable example is the optimization of water management through modifications of the electrodes' fine structures, allowing precise control of the hydration of the PEM and ionomer and thereby enabling a more reliable cell performance [9]. Although these improvements have positively impacted operational routines, the application in PEMFC systems continues to reveal the existence of yet unidentified sources for performance loss. That especially applies to the process of activating PEMFCs. The activation protocols often involve cycling of either temperature, voltage, humidity, or combinations of these parameters to break in the fuel cell and ultimately improve initial performance [10], but what exactly is causing the performance increase upon activation of PEMFCs is often unclear. This is partly based on the fact that many studies focus on single components and often neglect the interactions between them, meaning that investigations of such interfacial interactions remain an underexplored area.

Beyond initial performance optimization, ensuring long-term durability remains another critical challenge for PEMFC technology. Despite the operational excellence and stability of individual components under harsh operating conditions, deactivation and degradation of PEMFC electrodes over time continue to limit operational lifetime and impede a broader commercialization of this technology [11]. A gradual decline in the performance of a PEMFC can occur through a range of various mechanisms, with a major contributor being the loss of catalyst material, such as platinum NP dissolution, migration, coalescence, and detachment, which significantly diminish the active surface area. These processes are either facilitated or induced by the corrosion of the carbon support material [12–17]. Degradation is, however, not confined only to the catalyst and support. A further key factor is the deterioration of the PEM or ionomer material, driven in part by the formation of hydrogen peroxide within the fuel cell at cathode potentials below 0.696 V vs. the standard hydrogen electrode or as a result of oxygen crossover to the anode [18, 19], leading to reactive radical species attacking the side chains or terminal groups of the polymer backbone, and ultimately degradation of PFSA polymer [20–22]. Comparable damage can furthermore arise from electrochemical and mechanical stress associated with hydration cycling [23], where repeated changes of the structure within the material lead to internal stresses and embrittlement. When the polymer structure deteriorates, proton conductivity between anode and cathode is impaired, causing a progressive increase in the intrinsic ohmic resistance of the fuel cell. However, also in degradation studies these mechanisms are often examined at the level of individual components, frequently overlooking the complex interactions at material interfaces. Yet, these interfacial phenomena likely play a decisive role in both activation behavior and long-term degradation, and remain insufficiently understood.

In particular, little is known about the interactions between the ionomer and the catalytic platinum NPs or carbon support within the CL. Due to the complexity of this system, computational studies are a common means of gaining an understanding of the prevailing interfacial conditions. Several of these studies predict the formation of an interfacial water layer, where the equilibrium state of the interfacial water molecules critically influences the morphology of the ionomer at this interface [24, 25]. Further work has also shown that the local electrode potential plays a crucial role in this context [26, 27]. In contrast, experimental studies have lagged behind. Several extensive studies have characterized the ionomer ex situ using techniques such as electron microscopy combined with X-ray spectroscopy, providing valuable insights into its morphology under controlled conditions [28, 29]. However, these approaches cannot capture the dynamic structural changes that occur during operation. To address this, in situ methods like atomic force microscopy (AFM) measurements have been explored and were able to reveal a lamellar structure of the ionomer film in the CL of a membrane electrode assembly after testing [30]. Yet, there is still a lack of experimental investigations on how changes in electrode potential affect the morphology of the ionomer material.

An alternative in situ technique to AFM for probing morphological changes is the quartz crystal microbalance with dissipation monitoring (QCM-D). This method tracks shifts in frequency and energy dissipation of a quartz crystal oscillating at resonance. Changes in resonance frequency can be correlated with mass variations at the electrode, while the dissipation describes the amount of energy dissipated due to damping of the quartz crystal oscillation. The magnitude of dissipation is typically determined from the decay time of an induced oscillation. Finally, the combined observation of frequency and dissipation changes allows conclusions to be drawn about the viscoelastic properties of the electrode. Therefore, QCM-D has become a widely used tool in biological and polymer science to characterize thin films on sensor surfaces [31, 32]. When coupled with electrochemical measurements (electrochemical quartz crystal microbalance with dissipation monitoring, EQCM-D), this approach enables the analysis of potential-dependent processes and their effects on surface characteristics. This technique has been employed in earlier studies to investigate, for example, the Pt/electrolyte interfaces in different electrolytes [33, 34] as well as the impact of potential changes on the dissolution behavior of platinum electrodes in both acidic and alkaline environments [35, 36]. Further it also has been used to examine the catalytic role of platinum NPs in accelerating the corrosion of carbon electrodes [37]. Other previous EQCM studies have elucidated the potential–dependent adsorption and desorption of perfluorosulfonated ionomers on noble metal electrodes from solution [38, 39]. However, the dynamic interaction of a predeposited ionomer thin film in direct contact with platinum and carbon electrodes under electrochemical cycling conditions remains insufficiently characterized, particularly with respect to the ionomer's structural evolution and hydration state.

In this work, EQCM-D measurements were performed during cyclic voltammetry (CV) on platinum, carbon, and gold electrodes coated with a 30 nm Nafion layer to investigate the influence of electrode material and electrolyte composition on the interfacial behavior of ionomer films. Experiments were carried out in both 0.5 M H_2SO_4 and 0.1 M $HClO_4$ under otherwise identical conditions, as these acids and concentrations are commonly employed in the evaluation of PEMFC catalysts in half-cell setups. This choice was made to ensure an applicable and meaningful comparison with literature data and practical catalyst testing environments. The results reveal that the viscoelastic properties of the Nafion film exhibit dynamic responses to potential cycling. This response indicates the polymer film's sensitivity to potential-induced modifications of the electrode/ionomer interface, particularly the surface state of the electrode during oxidation and reduction. In the case of measurements on platinum electrodes in H_2SO_4, repeated potential cycling led to a pronounced increase in polymer hydration, suggesting dynamic changes in interfacial structure as a driving factor. In contrast, distinct responses in $HClO_4$ underline the influence of the electrolyte composition on the structural response of the ionomer layer. To assess the relevance of these findings to practical fuel cell electrodes, additional measurements were performed on spray-coated PEMFC electrodes. The observed potential-dependent hydration dynamics closely mirrored those of a planar Nafion-coated electrode, thereby implying that the same structural changes in the ionomer film are likely to occur in real fuel cell electrodes as a result of the surface reactions on platinum in response to potential variation. Moreover, these results demonstrate that EQCM-D is a relevant tool for providing mechanistic insights into ionomer behavior within practical electrode architectures.

2 | Results and Discussion

2.1 | EQCM-D Measurements in H_2SO_4

Figure 1 shows the data from CV alongside the corresponding mass and dissipation changes measured simultaneously via QCM-D for three different electrode materials. Electrodes of platinum, carbon, and gold were tested, each with and without an additional Nafion coating. The Nafion coating was applied by spin coating and the thickness and homogeneity of the coating was checked by a surface profiler, AFM, and optical microscopy (more detailed information can be found in the Supporting information). All data was recorded at 25°C in 0.5 M H_2SO_4 with a scan rate of 50 mV s^{-1}. Since a detailed comparison between the cases with and without Nafion across the different electrode materials is not the primary focus of Figure 1, we refer interested readers to the Supporting Information, where an additional plot is provided that specifically highlights these differences providing data for in-depth analysis. The mass changes reported throughout refer to the Sauerbrey mass, calculated using the Sauerbrey equation in liquid medium [40].

For the Pt-only electrode (Figure 1a), the characteristic electrochemical behavior of polycrystalline platinum surfaces and the associated potential-dependent mass and dissipation changes are in good agreement with previous reports [36, 41]. The mass response observed during CV can be divided into four key regions: (i) hydrogen interaction (0.05–0.4 V vs. reversible hydrogen electrode, RHE), (ii) double-layer charging (0.4–0.6 V vs. RHE), (iii) OH adsorption and platinum oxidation during the forward scan (starting at ~0.8 V vs. RHE to 1.25 V vs. RHE), and (iv) platinum oxide reduction during the reverse scan (1.25–0.6 V vs.

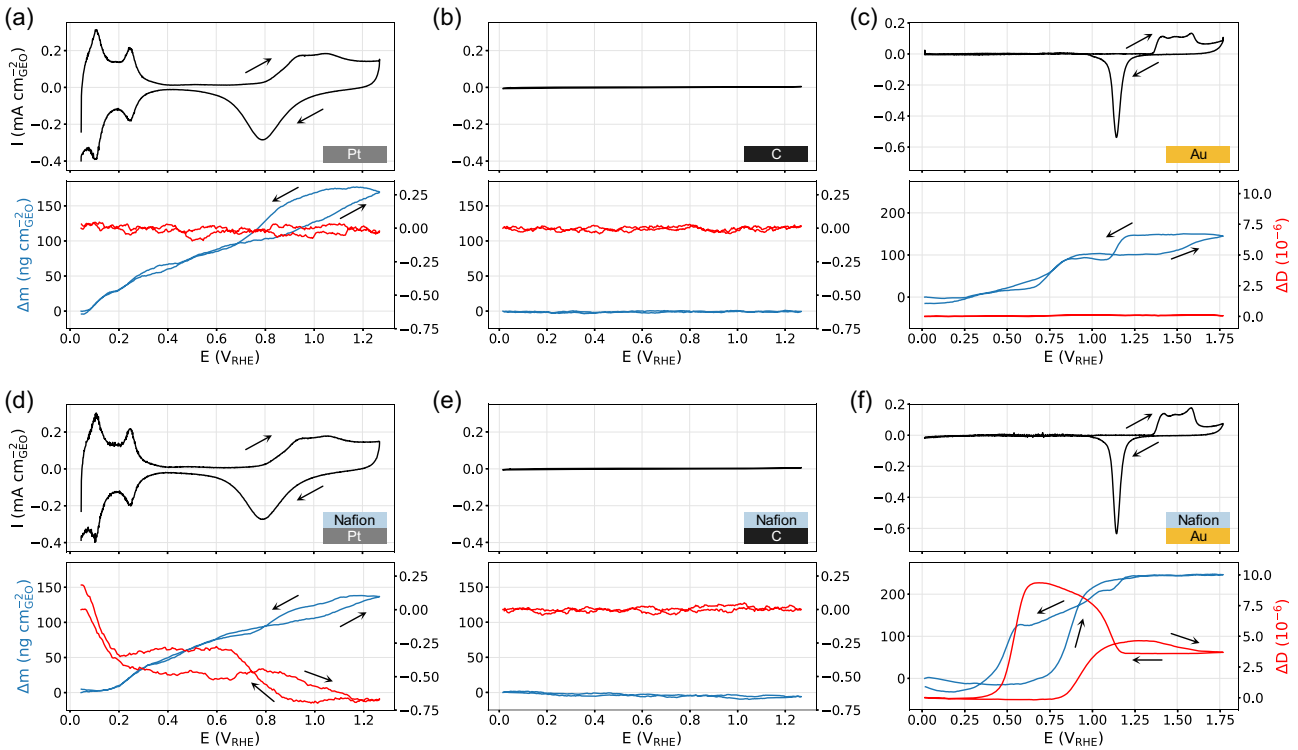

FIGURE 1 | Comparison of CV (black), Sauerbrey mass (blue), and dissipation (red) response during EQCM-D measurements of platinum, carbon, and gold electrodes with and without an approximately 30 nm thin layer of Nafion. The measurements were performed at 25°C in 0.5 M H_2SO_4 with a scan rate of 50 mV s^{-1}. In the upper row, (a) presents the data for the Pt-only electrode, (b) for the C-only electrode, and (c) for the Au-only electrode. In the lower row, (d) shows the data for the Pt/Nafion electrode, (e) for the C/Nafion electrode, and (f) for the Au/Nafion electrode.

RHE). Each region of the mass response thereby reflects distinct surface processes, including (i) displacement of interfacial water during hydrogen adsorption [42, 43], (ii) gradual mass increase due to anion and water coadsorption [34], and mass changes associated with (iii) oxide formation and (iv) reduction. A minor net mass loss is observed when comparing the Sauerbrey mass signal at the beginning and the end of the cycle at the same potential (−0.05V vs. RHE), caused by platinum dissolution occurring mainly during the platinum oxide reduction [44]. No significant changes in the dissipation of the quartz crystal oscillation were detected throughout the scan, indicating negligible changes in the viscoelastic properties of the surface, which in this case can be interpreted as no changes in the platinum surface structure, i.e., roughness [45].

For the C-only electrode, very small electrochemical currents corresponding to capacitive charging/discharging of the electrochemical double layer and virtually no relevant changes in the resonance frequency or dissipation can be detected within the tested potential range (Figure 1b). This observation aligns with earlier studies reporting that surface redox processes, such as the reversible conversion between hydroquinone and quinone groups, may occur below 1.35 V vs. RHE, but their electrochemical and gravimetric signatures are minimal compared to the prominent features observed for metal electrode surfaces [46].

For the Au-only electrode (Figure 1c), the mass and dissipation response was recorded over the extended potential range from 0.05 to 1.8 V vs. RHE. This potential window was selected for all gold electrode measurements in this study to encompass both oxidative and reductive conditions relevant to gold surface processes (results for EQCM-D measurements recorded in a similar potential range as for the measurements of the Pt-only electrodes, namely 0.05–1.25 V, can be found in the Supporting Information). The aim was to investigate the response of a Nafion film during electrochemical reactions on another noble metal surface to enable comparison with the behavior observed for the Pt/Nafion electrode. The mass response of the Au-only electrode can be categorized into three main regions [47, 48]: (i) double-layer charging (0.3–1.0 V vs. RHE), (ii) anodic oxidation of the gold surface (1.0–1.8 V vs. RHE), and (iii) subsequent oxide reduction (1.8–1.0 V vs. RHE). (i) In the double-layer region, a continuous increase in mass is observed, attributed to the strong specific adsorption of sulfate and bisulfate anions along with the coadsorption of water molecules. (ii) Upon the onset of gold oxidation, the mass increases further, reflecting the formation of hydrated gold oxide species. (iii) During the reduction phase, the mass decreases gradually as the oxide is reduced, with the process being largely reversible.

Figure 1d–f displays CV, Sauerbrey mass and dissipation response for the three different electrode materials after each was coated with an approximately 30 nm thin layer of Nafion. Compared to Figure 1a–c, it becomes evident that the voltammograms do not differ significantly, suggesting that the electrochemical processes occurring at the electrode surface are not substantially affected by the presence of a thin Nafion layer. In contrast, the mass and dissipation responses exhibit pronounced differences.

For the Pt/Nafion electrode (Figure 1d), the general characteristics of the potential-dependent mass changes are still observable. However, the hysteresis between mass increase due to oxidation and mass decrease due to reduction of the platinum surface appears smaller compared to the Pt-only electrode. The specific potential at which the mass change occurs does not shift noticeably, but rather magnitude of the mass change is reduced. More precisely, the increase in Sauerbrey mass due to oxidation of the platinum surface appears to be approximately 30 ng cm^{-2} lower for the Pt/Nafion electrode compared to the Pt-only electrode. Accordingly, the mass loss during the reduction of the platinum oxide surface is also slightly reduced compared to the case without Nafion. While these differences are relatively small, they are systematic and reproducible across multiple cycles during CV after conditioning of the electrode surface. Additional details and supporting data are provided in the Supporting Information.

We hypothesize that the sulfonic acid groups of the ionomer influence the structure of the water–platinum interface during the platinum oxidation. Previous studies have demonstrated that the hydrophilic side chains of the ionomer can disrupt the structure of the electrical double layer at the water–platinum interface [38, 49, 50], thereby reducing both the density and adsorption of water at this interface [43, 51]. It is therefore reasonable to assume that this disruption of the double layer has a significant local influence on the morphology of the water coupled to the oxidized platinum surface. In previous studies, it has been shown that electrode surfaces can undergo pronounced roughening during oxidation, which typically leads to an overestimation of the mass change at the electrode surface in EQCM measurements based on the shift in resonance frequency [52, 53]. A substantial portion of the observed mass change arises from water being trapped within cavities of the roughened, oxidized surface. At this stage, it appears plausible that the presence of the Nafion layer, along with its interaction with the metal surface, contributes to a partial suppression of the surface roughening effect and water trapping.

The so-called Gibbs–Donnan effect might provide another potential reason for the observed behavior [54]. This effect describes the presence of an electrostatic barrier within a polymer film caused by fixed charged groups. In the specific case of Nafion, the negatively charged sulfonate groups in the hydrated state must be balanced by positively charged ions. This leads to an unequal distribution of ions between the polymer phase and the bulk electrolyte, creating an electrostatic potential at the polymer–electrolyte interface [55, 56]. Such a potential can act as a barrier for anions, making it more difficult for, e.g., sulfate ions from the electrolyte solution to migrate through the polymer film. It is therefore probable that this effect also impedes the specific adsorption of sulfate ions, which could manifest as the reduced mass increase during oxidation, and consequently, the diminished hysteresis. This assumption is supported by the observation that specific adsorption of sulfate ions can contribute to an overestimation of mass increase in EQCM-D measurements of this system [34].

An alternative or complementary explanation, however, may be found in the changes in viscoelastic properties of the Nafion layer itself, which becomes apparent upon closer inspection of the dissipation signal. Particularly striking in this regard is the strong potential dependence observed in the measured dissipation changes on the Pt/Nafion electrode (Figure 1d). While on the Pt-only electrode (Figure 1a), the dissipation is constant during cycling, a Nafion film on platinum causes the dissipation to clearly change during the cycle and the response can be divided

into four regions: in the range of approximately 0.05 to 0.2 V vs. RHE (i), there is a pronounced decrease in dissipation, which then stabilizes in the range of 0.2 to 0.8 V vs. RHE (ii). Subsequently, a further decrease in dissipation is observed between about 0.8 and 1.25 V vs. RHE (iii). During the cathodic scan, an increase in dissipation is apparent in the range from 1.25 to 0.6 V vs. RHE (iv), and it is noteworthy that this increase is not reversible, as it significantly exceeds the initial level. It is also striking that these changes in the dissipation of the quartz crystal oscillations closely correlate with certain features of the CV. Region (i) appears to coincide with the first hydrogen adsorption peak, (ii) represents the double-layer region up to Pt oxidation, and (iii) as well as (iv) correspond to subsequent oxidation and reduction processes, respectively. Since measurements on a C/Nafion electrode (Figure 1e) do not exhibit any comparable features, it can be ruled out that the observed dissipation changes in Figure 1d are due to a potential-dependent response of the Nafion layer itself. Instead, it appears that the Nafion layer responds directly to electrochemical reactions or changes on the platinum surface and the water–platinum interface during measurements.

We argue that in the case of a Pt/Nafion electrode the most plausible explanation is that the changes in dissipation during CV are attributed to structural changes in the Nafion layer and likely also an increased water uptake in the Nafion, arising from the diffusion of water molecules and sulfate ions to and from the platinum surface as a result of the electrochemical processes on the platinum surface. This interpretation is primarily based on the well-established observation that the dissipation of quartz crystal oscillations in QCM measurements of polymer films is highly sensitive to changes in hydration [57]. A variation in the water content of a polymer film alters its viscoelastic properties: a film with lower water content behaves more rigidly with respect to oscillatory motion compared to a respective film with higher levels of trapped water. This change in shear modulus of the polymer layer directly affects the damping of the oscillation of the quartz crystal, which in turn is expressed through the dissipation signal [31, 45, 58]. Consequently, dissipation responds strongly to variations in the viscoelastic properties of the film, which scale with the polymer's water content [59, 60]. During the oxidation of the platinum surface, which can be described as [61]

$$Pt + H_2O \rightarrow PtOH_{ads} + H^+ + e^- \quad (1)$$

$$PtOH_{ads} \rightarrow PtO + H^+ + e^- \quad (2)$$

$$PtO + H_2O \rightarrow PtO_2 + 2H^+ + 2e^- \quad (3)$$

Water molecules are consumed from the interfacial region, effectively lowering the water content within the adjacent Nafion layer, while at the same time protons are generated which will be solvated by additional water molecules to form the well-known hydration shell structure [62]. This results in a stiffening of the layer, reflected by a decrease in dissipation in region (iii). This reduction in water content within the Nafion layer and its surrounding environment may also offer an explanation for the previously noted discrepancy in mass increase of approximately 30 ng cm^{-2} observed during surface oxidation between the Pt-only and Pt/Nafion electrodes. More precisely, a portion of the water participating in the oxidation reaction may already be confined within the Nafion layer and thus mechanically coupled to the oscillation of the quartz crystal prior to the onset of oxidation. As a result, the additional water mass detected during the reaction appears smaller compared to the Pt-only electrode, where all water involved originates from the bulk electrolyte and contributes more directly to the observed mass change. Conversely, during the subsequent reduction of the oxide layer (region iv), water is released back into the surrounding Nafion, increasing its hydration and thereby its viscosity, which manifests as an increase in dissipation. The irreversibility of this response of the Nafion film on a platinum surface to interfacial electrochemical reactions can be explained by the net water transport during the oxidation step. Water and anions appear to diffuse along the gradient through the Nafion layer toward the electrode surface to maintain ionic coordination in the electrolyte [63]. However, not all of this water seems to be expelled from the polymer matrix during the reverse (reductive) process, resulting in a net increase in mass due to an increased water content in the Nafion film.

A similar behavior is observed for the Au/Nafion electrode (Figure 1f). In the oxidation region (1.35–1.65 V vs. RHE), a pronounced decrease in dissipation is evident, while in the reduction region (1.25–1.00 V vs. RHE), a strong increase in dissipation occurs. In this case as well, the dissipation rises significantly above the initial value following reduction. However, additional pronounced dissipation changes are observed in the double-layer region. During the anodic scan, a distinct increase in dissipation begins at approximately 0.8 V vs. RHE. During the cathodic scan, immediately following the reduction of the gold oxide surface (below 1.0 V vs. RHE), a slightly weaker increase in dissipation is seen, followed by a sharp drop at applied potentials below 0.6 V vs. RHE. At low applied potential, the dissipation returns to its initial value, suggesting that the dissipation changes during a single CV cycle are fully reversible.

The response of the dissipation to the oxidation and reduction of the gold surface closely resembles that of the Pt/Nafion electrode, although appearing significantly more pronounced, and can be similarly explained by a depletion of interfacial water and subsequent stiffening of the Nafion layer during oxidation, as well as rehydration and increased viscosity during reduction according to:

$$2Au + 3H_2O \rightarrow Au_2O_3 + 6H^+ + 6e^- \quad (4)$$

The behavior in the double-layer region, on the contrary, differs significantly from that of platinum. In the case of the Au/Nafion electrode, substantial dissipation changes are observed in this region, in some cases exceeding those caused by electrochemical reactions happening at the metal surface. These dissipation changes can be explained by the distinct nature of interfacial processes occurring at gold electrodes in sulfuric acid between 0.05 and 1.2 V vs. RHE. Under these conditions, adsorption of sulfate anions and coadsorption of water molecules take place. The formation of hydrogen bonds between sulfate ions and water leads to the development of highly ordered adsorbate layers at the electrode surface [64, 65]. Ataka et al. [66] reported a potential-dependent restructuring of these adlayers, identifying two characteristic potentials at which the interfacial water layer undergoes significant rearrangement. These structural changes occur at electrode potentials around 0.5 and 0.8 V vs. RHE. In our experiments, we also observed dissipation changes at these

potentials, which we attribute to the response of the Nafion layer to restructuring of the adsorbed sulfate/water layer at the gold surface.

A direct comparison between measurements on gold electrodes with and without Nafion reveals that the frequency change stemming from the mass increase typically associated with the formation of surface oxides during the anodic scan is significantly attenuated by the polymer layer. Specifically, in the potential range between 1.25 and 1.75 V vs. RHE, no measurable mass change is detected. This behavior mirrors previous observations made for platinum electrodes, where a diminished mass response was attributed to Nafion-induced alterations of the metal surface properties, most likely through specific interactions at the polymer–electrode interface, or to the partial preconfinement of reactive water within the Nafion layer, which is already mechanically coupled to the QCM sensor prior to the onset of oxidation. In the case of gold, an additional contribution may stem from enhanced dissolution of gold or the partial desorption of specifically adsorbed sulfate anions during the anodic process. This would result in a compensating mass loss that counteracts the expected mass gain due to oxide formation, thus leading to an apparent net-zero mass change within this potential window. In a similar way, the previously discussed Donnan-effect might contribute by limiting the accessibility of sulfate ions to the gold surface, thereby reducing their specific adsorption in a manner similar to what was described for platinum electrodes. Moreover, during the cathodic scan, the decrease in Sauerbrey mass proceeds only gradually once the electrode potential drops below 1.25 V vs. RHE. A pronounced mass loss is observed only at potentials more negative than 0.5 V vs. RHE, which coincides with a sharp reduction in dissipation. This behavior strongly suggests that, between 1.25 and 0.5 V vs. RHE, additional water remains trapped within the interfacial region of the crystal and remains coupled to its oscillation. The final release of this water appears to be associated with the potential-driven reorganization of the electrical double layer at the gold surface, which likely disrupts the hydrogen-bonding network and enables water expulsion from the Nafion matrix.

To illustrate the differences between measurements on electrodes without and with Nafion, Figure 2 shows plots of the Sauerbrey mass change versus charge, following the approach used in previous studies [34, 67]. The plotted data correspond to the forward scan of the EQCM-D measurements shown in Figure 1. For the Pt-only electrode (Figure 2a, dark blue curve), the plot can be divided into four distinct regions, each associated with specific electrochemical surface processes: The linear trend observed in Region (i) is attributed to the desorption of adsorbed hydrogen atoms from the platinum surface. The positive mass change has been investigated in previous studies and explained by a gradual increase in water molecule adsorption on the platinum surface as hydrogen atoms desorb [33, 34]. A similar effect is observed during double-layer charging, represented by Region (ii). In this region, the steep slope indicates a significant mass increase with only minimal charge transfer, which is likewise explained by additional water adsorption at the surface [36]. Some studies also consider the possible contribution of adsorption of anions from the electrolyte solution [34, 67]. In region (iii), the slope of the curve decreases markedly as oxidation of the platinum surface begins, resulting in substantial charge transfer. Jerkiewicz et al. proposed a two-step oxidation mechanism [36]: (1) partial discharge of the adsorbed water layer accompanied by chemisorption of oxygen on the platinum surface; (2) discharge of the remaining part of the water monolayer, during which chemisorbed oxygen atoms undergo interfacial site exchange due to repulsive dipole–dipole interactions, leading to the formation of a PtO lattice on the electrode surface. The second step of this oxidation process is represented by Region (iv) in the plot. While Jerkiewicz et al. excluded sulfate anion interactions during oxidation [36], other studies interpret discrepancies in mass increase as a contribution from specific anion adsorption from the electrolyte [67]. Given the slight variations in previously reported mass changes across these regions, we do not discuss detailed adsorption mechanisms here. Instead, we note that the mass changes observed in our study relative to the transferred charge are in good agreement with previously reported data [34, 36, 67].

More interesting, however, is how this relationship changes in the presence of a Nafion film. The data for the Pt/Nafion electrode are shown in light blue in Figure 2a and generally exhibit a similar overall trend to the Pt-only electrode, but with notable

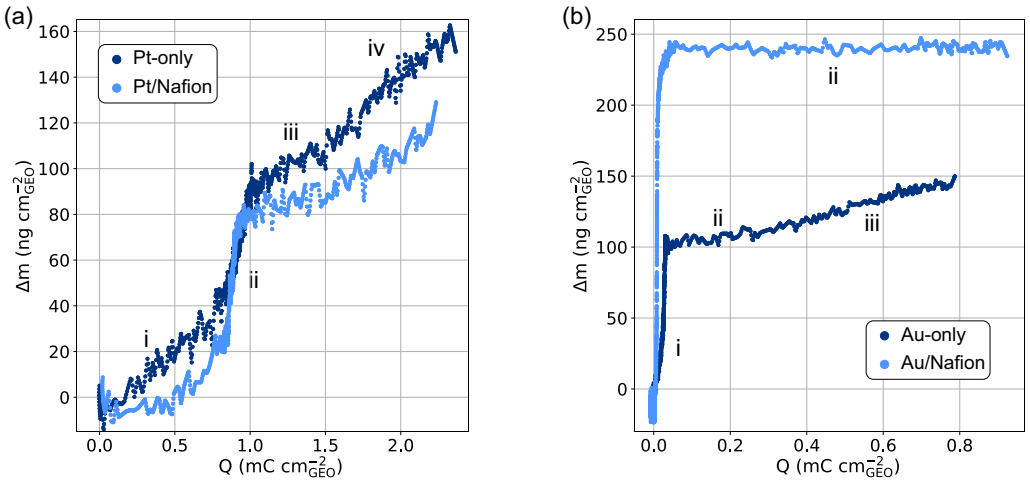

FIGURE 2 | Comparison of Sauerbrey mass change vs. charge plots for (a) Pt-only and Pt/Nafion electrodes, and (b) Au-only and Au/Nafion electrodes during a CV in at 25°C in 0.5 M H_2SO_4 with a scan rate of 50 mV s^{-1}. The plots were obtained from the data shown in Figure 1 during the respective forward scan.

differences in specific regions: In Region (i), the curve for the Pt/Nafion electrode is not linear. In the start of Region (i), the Sauerbrey mass changes very little, but toward the end of the region, the mass change increases progressively with transferred charge, reflected in the steepening slope. This suggests that the mechanism during hydrogen desorption differs from that of the Pt-only electrode and that water adsorption does not proceed in the same manner. As discussed earlier, this is likely due to interactions between the polymer film and the interfacial water layer [25–27]. In Region (ii), so the double-layer charging region, the slope for the Pt/Nafion electrode is higher than for the Pt-only electrode. Since this region is associated with water (and possibly anion) adsorption, it is reasonable to assume that the Nafion film influences the composition of the adsorption layer. Adsorption of sulfonate groups and resulting conformational changes of the polymer film cannot be excluded [39]. In Regions (iii) and (iv), the lower slope for the Pt/Nafion electrode compared to the Pt-only electrode indicates a smaller increase in Sauerbrey mass during platinum surface oxidation. This effect, previously discussed in relation to Figure 1, can likely be explained by the following factors: consumption of water molecules from the overlying Nafion layer, which due to trapping in the polymer were already coupled to the quartz crystal oscillation prior to oxidation, and possible inhibition of sulfate ion adsorption from the solution due to the Donnan effect, reducing mass increase and thus the slope. The exact cause remains speculative, as the interpretation of Sauerbrey mass changes is limited by simultaneous changes in dissipation. Consequently, frequency shifts, and thus changes in Sauerbrey mass, must be interpreted in terms of changes in the viscoelastic properties of the electrode [31, 45, 58]. Therefore, the Sauerbrey mass changes only indirectly reflect electrochemical processes, complicating the identification of adsorbed species.

Figure 2b shows the corresponding plots of change in Sauerbrey mass versus transferred charge for gold electrodes, with the Au-only electrode represented in dark blue and the Au/Nafion electrode in light blue. The curve for the Au-only electrode can be divided into distinct regions similar to platinum, although in this case only three clearly different regions are observed, as no electrochemical processes related to hydrogen desorption occur on the gold surface. Region (i) corresponds to the double-layer charging, where the mass increases due to adsorption of sulfate ions and water molecules, while only minimal charge transfer is observed. Regions (ii) and (iii) both exhibit lower slopes compared to Region (i), with Region (iii) showing a steeper slope than Region (ii). This behavior essentially mirrors that of the Pt-only electrode during surface oxidation and can therefore be interpreted in a similar manner. Overall, the trend observed for the Au-only electrode is in good agreement with previous studies [68, 69].

The difference in curve profile for the Au/Nafion electrode, however, is substantial. Here, only two regions can be identified: Region (i), representing the double-layer charging, and Region (ii), corresponding to the oxidation of the electrode surface. Notably, no mass change is observed during the entire oxidation process. In contrast, the mass increase in Region (i) is significantly larger than for the Au-only electrode. This observation, previously discussed in relation to Figure 1, can be interpreted in several different ways. It is reasonable to assume that the presence of the Nafion layer alters the interactions of water and anions, thereby influencing their adsorption at the surface. The Donnan effect may also play a role. Additionally, the mass change is likely affected by the fact that part of the reacting water is already coupled to the quartz crystal oscillation through trapping in the Nafion film prior to oxidation. As in the platinum case, it is important to note that simultaneous changes in Sauerbrey mass and dissipation indicate that the observed mass change may be only indirectly related to electrochemical processes and is also influenced by variations in viscoelastic properties.

The presented results demonstrate that the ionomer film deposited on the electrodes is significantly influenced by potential-dependent structural changes occurring both at the electrode surface and within the electrical double layer. These changes lead to pronounced fluctuations in the viscosity and therefore hydration state of the Nafion film. While these fluctuations appear to be reversible in the case of Nafion on gold, Nafion on platinum exhibits irreversible behavior, with dissipation ending up at a higher value by the end of each CV cycle compared to its beginning. To better visualize these changes in mass and dissipation between CV cycles, Figure 3 presents the evolution of both parameters over the course of ten consecutive CV cycles. The data points were recorded at the end of each cycle, where one cycle is defined as a full potential sweep from 0.05 to 1.25 V vs. RHE and back. For clarity and ease of comparison, the graphs are arranged in the same layout as in Figure 1. Figure 3a–c shows the reference measurements for the three electrode materials without an additional ionomer layer, while Figure 3d–f displays the corresponding measurements for electrodes coated with a Nafion layer. All experiments were conducted under the same conditions as those described for Figure 1.

The dissolution behavior of the Pt-only electrode is presented in Figure 3a. The data reveal that, under CV conditions with an upper potential limit (UPL) of 1.25 V vs. RHE, the electrode experiences a consistent mass loss of approximately 7.5 ng cm^{-2} per cycle, indicating platinum dissolution. This finding is in excellent agreement with prior literature, which has established that the majority of platinum dissolution occurs during the cathodic sweep, specifically during the reduction of the surface oxide layer, at potentials near 0.8 V vs. RHE [35, 44].

A similar trend of metal dissolution is observed for the Au-only electrode (Figure 3c) during CV with an UPL of 1.8 V vs. RHE, although the extent of material loss is substantially greater, averaging approximately 15 ng cm^{-2} per cycle. This elevated dissolution rate is consistent with previous studies and is attributed to the distinct electrochemical behavior of gold at high potentials [70]. In contrast to platinum, gold dissolution was shown to occur not only during the cathodic sweep but also during the anodic scan at potentials exceeding 1.6 V vs. RHE [70, 71]. This process is further facilitated by the formation of soluble gold–sulfate adsorbates, which accelerate the rate of metal loss and account for the observed discrepancy between the two noble metals [72].

As expected, C-only electrodes exhibit no significant mass changes over successive cycles (Figure 3b), as no significant faradaic processes involving the electrode material occur under the applied conditions. Consequently, the EQCM-D signal remains stable throughout the CV scans. Moreover, across all three electrode materials, the dissipation signal remains essentially unchanged over the course of the ten consecutive CV cycles, indicating that the viscoelastic properties at the electrode interface are not significantly altered during the electrochemical processes described above.

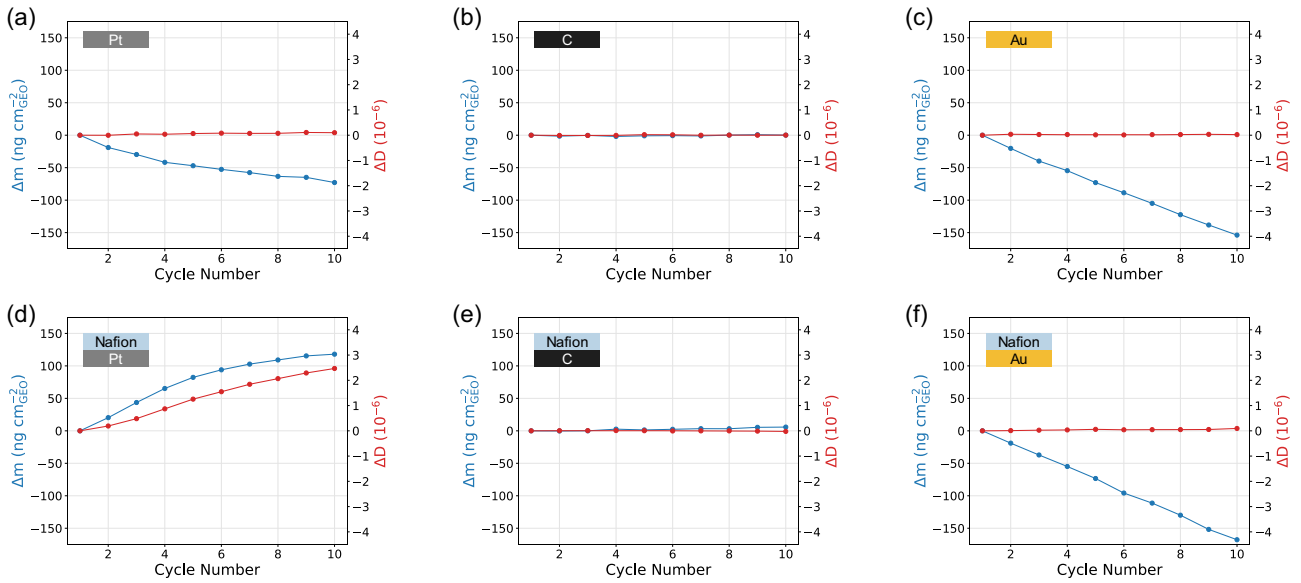

FIGURE 3 | Comparison of Sauerbrey mass (blue) and dissipation (red) change over 10 CV cycles during EQCM-D measurements of platinum, carbon and gold electrodes with and without an approximately 30 nm thin layer of Nafion. The measurements were performed at 25°C in 0.5 M H_2SO_4 with a scan rate of 50 mV s^{-1} and the data points were taken at the end of each cycle (one cycle is defined as a full potential sweep from 0.05 to 1.25 V vs. RHE and back). The potential range for measurements on platinum and carbon electrodes covered 0.05–1.25 V vs. RHE and on gold electrodes 0.05–1.8 V vs. RHE. In the upper row, (a) presents the data for the Pt-only electrode, (b) for the C-only electrode, and (c) for the Au-only electrode. In the lower row, (d) shows the data for the Pt/Nafion electrode, (e) for the C/Nafion electrode, and (f) for the Au/Nafion electrode.

However, the observed response changes markedly upon the addition of a Nafion layer to the electrodes. On the Pt/Nafion electrode (Figure 3d), the presence of the ionomer significantly affects both the dissipation and the Sauerbrey mass response. Over the course of ten consecutive CV cycles, a continuous increase in the measured mass is observed, eventually reaching a plateau between cycles 8 and 10, with a total mass gain of approximately 105 ng cm^{-2}. The dissipation signal exhibits a similarly pronounced trend, culminating in a total increase of 2.4×10^{-6} after ten cycles. Notably, the most substantial changes in both mass and dissipation occur within the first five cycles. The underlying mechanisms are consistent with those discussed earlier. Specifically, the concurrent increase in mass and dissipation can be interpreted as a change in the viscoelastic properties of the Nafion film due to enhanced water uptake. Again, this interpretation is based on the principle that simultaneous changes in dissipation and Sauerbrey mass during QCM-D measurements can be linked to variations in the viscoelastic properties of the electrode [31, 45, 58]. For polymer films in particular, an increase in both dissipation and Sauerbrey mass is commonly associated with enhanced viscoelasticity resulting from an increased amount of water trapped in the polymer matrix [59, 60]. As described earlier, these modulations in viscoelasticity occur dynamically during individual CV cycles and correlate with the oxidation and reduction processes at the metal electrode surface. Importantly, these changes are partially irreversible, leading to a cumulative shift in both dissipation and Sauerbrey mass over multiple cycles. This net change in mass and dissipation reflects a net alteration in the viscosity of the Nafion layer, consistent with a net change in hydration of the polymer film. Therefore, these observations suggest that the repeated oxidation and reduction of the platinum surface exerts a 'pumping' effect on water within the ionomer layer. In turn, this results in amplified hydration of the Nafion film beyond its initial state. The additional water becomes sterically confined within the film and is thus coupled to the oscillation of the quartz crystal, registering as a Sauerbrey mass increase. This amplified hydration is most pronounced during the first five cycles, after which the mass and dissipation changes approach a steady state, indicating that an equilibrium in the water content of the Nafion film is reached relatively early during cycling. Here, it should be mentioned that the mechanisms discussed may also compete with other processes occurring over longer timescales in polymers of this type. Although not clearly evident from the present data, platinum dissolution is likely taking place. Dissolved Pt ions can become trapped within the polymer matrix, as reported in previous studies on aging of Nafion membranes [73]. Such incorporation of metal ions would ultimately lead to a progressive stiffening of the polymer through physical cross-linking.

The results presented here are particularly intriguing in the context of PEMFC activation protocols, which often involve deliberate potential cycling to improve cell performance [10]. While the exact mechanisms underlying PEMFC activation remain only partially understood, it is common to presume that the activation, among other aspects, improves the proton conduction in the CL, contributing to improved conductivity and overall performance. This activation of the polymer material is thought to involve multiple processes, including hydration and structural reorganization of the polymer, reorientation at the ionomer-catalyst interface, and the removal of contaminants [10]. Of particular relevance to the present study is the role of hydration. During initial conditioning of the membrane or CL, water domains within the polymer matrix have been observed to expand, promoting increased proton transport [74, 75]. For instance, during hydrothermal treatment of PEMs, irreversible changes in their viscoelastic properties are commonly observed [76, 77]. These irreversible effects are typically attributed to morphological alterations within the membrane and the formation of more crystalline domains, leading to a more open porous structure and thereby providing more accessible pathways for migration of protons through the material

[78]. Thus, these previous observations with PEMs align very well with the type of behavior observed here via EQCM-D measurements. Consequently, the findings of this study may offer valuable mechanistic insights into the dynamics of Nafion hydration during PEMFC activation procedures.

The results obtained from measurements on a C/Nafion electrode are shown in Figure 3e. Similar to previous experiments on carbon electrodes, in this investigation, no significant change in the mass or dissipation of the electrode is observed, and both parameters remain largely constant over the course of ten cycles. These findings are consistent with earlier observations and lend further support to our hypothesis that the pronounced hydration of the Nafion film observed on platinum electrodes is a direct response of the polymer to electrochemical surface reactions at the platinum interface rather than a direct consequence of the applied potential. In the absence of such surface reactivity, as is the case for carbon electrodes, no significant restructuring or additional water uptake within the ionomer film is detected.

The final panel of Figure 3 (Figure 3f) presents the results of measurements conducted on the Au/Nafion electrode. A clear, approximately linear decrease in electrode mass is observed over ten CV cycles. The rate of Sauerbrey mass loss in this case is approximately 16 ng cm^{-2} per cycle, which is slightly higher than that observed for Au-only electrodes. The dissipation remains relatively constant throughout the cycling period. These findings indicate that the response of Au/Nafion electrodes closely resembles that of Au-only electrodes and contrasts distinctly with the behavior observed for platinum electrodes, where a clear reversal of the trends is observed between platinum electrodes with and without a Nafion layer. This discrepancy is, however, not unexpected, given that during voltametric cycling, the dissipation returns to its initial value at the end of each cycle, suggesting that Nafion on gold does not undergo the same water-pumping effect as observed on platinum. Consequently, there is no net increase in the hydration level of the polymer. Although the precise mechanism underlying this behavior cannot be directly deduced from the present data, we hypothesize that it is related to the pronounced response of the Nafion film to interfacial restructuring of the electrical double layer within the potential window between 0.3 and 1.0 V vs. RHE. As previously discussed, this restructuring may facilitate the expulsion of water from the Nafion matrix, thereby allowing the polymer film to revert to its initial hydration state. Additionally, the response of the electrode assembly is likely influenced by the presence of sulfate anions in the electrolyte. These anions exhibit a high affinity for gold surfaces and may mediate the dissolution of the gold electrode through the Nafion film. It is also important to note that the sulfonic acid groups in Nafion themselves possess a strong affinity for gold, thereby possibly contributing to the slightly increased dissolution rate observed in this configuration compared to gold-only electrodes. Together, these observations provide initial insights into the potential role of electrolyte anions and polymer–metal interactions in governing the behavior of Nafion films on metallic electrodes.

2.2 | EQCM-D Measurements in $HClO_4$

To further investigate the influence of the anions in the electrolyte solution on the mass and dissipation responses of the electrodes, additional experiments were conducted in 0.1 M $HClO_4$ using platinum and gold electrodes, both with and without a Nafion coating. Aside from the change in electrolyte, all measurements were performed under identical conditions to the previous experiments: at 25°C, using CV with a scan rate of 50 mV s^{-1}. The corresponding results from the EQCM-D measurements are shown in Figure 4. As with Figure 1, a version of Figure 4 that is better suited for in-depth comparison between the cases with and without Nafion is provided in the Supporting Information, for readers interested in examining the data more closely.

For Pt-only electrodes (Figure 4a), the typical electrochemical behavior of a polycrystalline platinum surface is observed. The mass response during a CV cycle can be interpreted analogously to the measurements conducted in H_2SO_4, as has been shown previously [35]. Notably, the dissipation remains constant throughout the entire CV cycle in perchloric acid, indicating no significant viscoelastic changes in the interfacial region.

A similar pattern is observed for Au-only electrodes, as shown in Figure 4b. From the data, the characteristic electrochemical behavior of a polycrystalline gold surface can be observed, with mass changes clearly tracking the faradaic processes occurring at the metal surface. As with the measurements of Au-only electrodes in H_2SO_4, the mass response can be divided into three regions: double-layer charging (0.3–1.0 V vs. RHE; i), anodic oxidation of the gold surface (1.0–1.8 V vs. RHE; ii), and subsequent reduction of the formed oxide (1.8–1.0 V vs. RHE; iii). It can be noted that no signs of specific adsorption of anions can be seen in the $HClO_4$ solution. This contrasts with the observations in H_2SO_4, and the behavior is attributed to the considerably weaker adsorption of ClO_4^--ions on polycrystalline gold surfaces compared to the stronger interaction with SO_4^{2-}-ions [79]. As a result, the mass response in the double-layer region in $HClO_4$ is more uniform. Likewise, the dissipation remains constant throughout the measurement, demonstrating no significant changes in the viscosity properties of the electrode during cycling.

While the responses of electrodes without a Nafion coating measured by EQCM-D in $HClO_4$ closely resemble those observed in H_2SO_4, substantial differences emerge in the behavior of electrodes coated with a Nafion layer. Figure 4c presents the EQCM-D results for a Pt/Nafion electrode in 0.1 M $HClO_4$. While the cyclic voltammogram exhibits the characteristic features of a polycrystalline platinum surface and shows no significant deviation from the response of a Pt-only electrode, the QCM-D signal reveals mass and dissipation changes that differ markedly from those observed in H_2SO_4. A pronounced peak in the Sauerbrey mass is detected in both scan directions within the potential range of 0.1–0.3 V vs. RHE. This is accompanied by a significant increase in dissipation. Above 0.3 V vs. RHE, however, the dissipation remains largely constant, while the mass signal shows the characteristic features associated with the oxidation and reduction of the platinum surface at potentials exceeding 0.6 V vs. RHE.

Similar to previous observations, the increase in mass and dissipation at low potentials can be associated with changes in the viscoelastic properties of the Nafion film on the electrode surface. The results here show that the interaction between the platinum surface and the polymer film is strongly influenced by the choice of electrolyte solution. The most apparent difference between perchlorate and sulfate anions lies in their valency and resulting charge density, which strongly influences their solvation behaviors in water [80–82]: SO_4^{2-}-ions, with their double negative charge, form strong

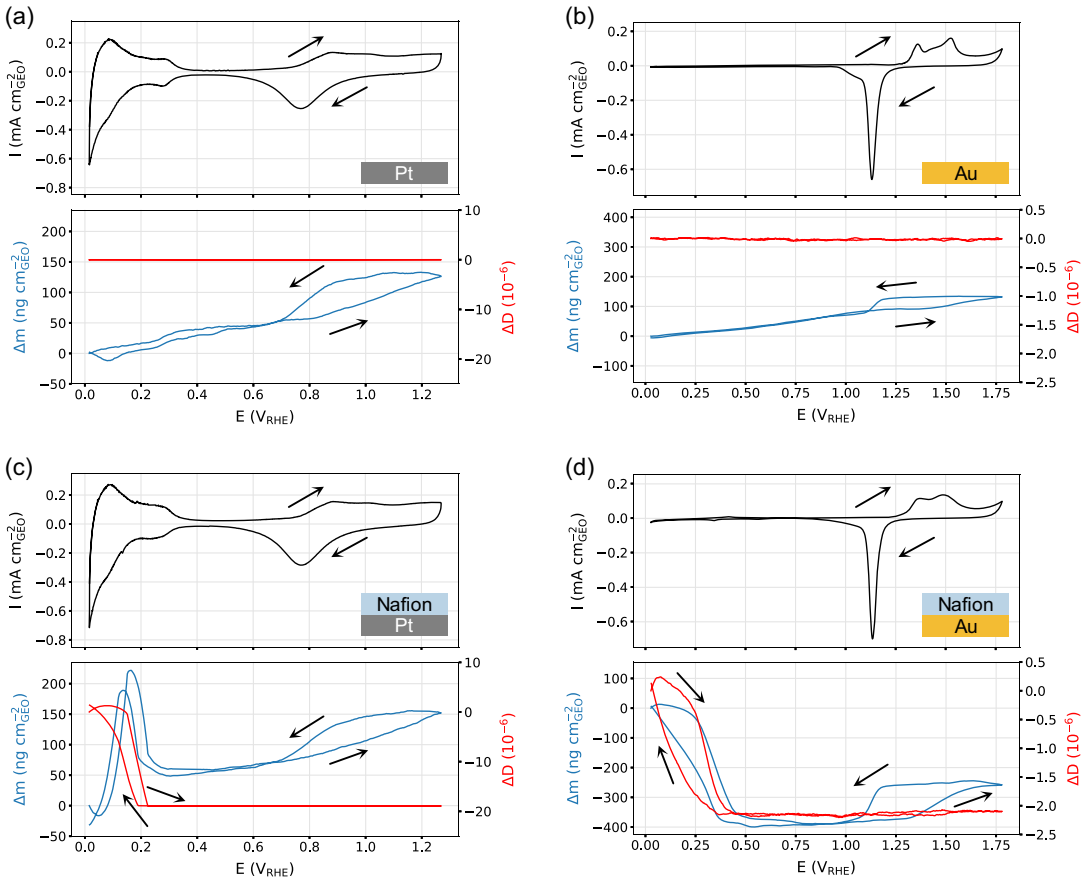

FIGURE 4 | Comparison of CV (black), Sauerbrey mass (blue), and dissipation (red) response 0.1 M $HClO_4$ during EQCM-D measurements of platinum and gold electrodes with and without an approximately 30 nm thin layer of Nafion. The measurements were performed at 25°C with a scan rate of 50 mV s^{-1}. In the upper row, (a) presents the data for the Pt-only electrode, and (b) for the Au-only electrode. In the lower row, (c) shows the data for the Pt/Nafion electrode, and (d) for the Au/Nafion electrode.

electrostatic interactions with water molecules, whereas ClO_4^--ions interact only weakly. Consequently, sulfate ions typically possess a solvation shell containing nearly twice as many water molecules compared to perchlorate ions. Moreover, sulfate ions act predominantly as kosmotropes, meaning they exhibit a strong organizing effect on the surrounding water structure. In contrast, perchlorate ions are generally chaotropic, which implies that they disrupt the typical water structure. These characteristics result in sulfate ions forming highly symmetric hydration shells, while perchlorate ions form markedly asymmetric ones.

Beyond their interactions with water, these ions also exhibit markedly different affinities for metal surfaces. For instance, sulfate ions are known to interact strongly with platinum surfaces, whereas perchlorate ions show only weak interactions [83]. Which of these effects primarily drives the trends observed in our measurements remains uncertain. Nevertheless, our data clearly demonstrates that when evaluating PEMFC catalysts, such as through rotating disk electrode measurements of catalysts with ionomer, the choice of electrolyte must be made with great care to ensure comparability of results. Although the electrochemical processes themselves do not appear to be significantly affected, non-faradaic processes and interactions between the various components can change substantially. These changes are difficult to discern from CV data alone and require more detailed insights into the electrode surface environment to be properly understood.

A comparable response is observed for the Au/Nafion electrode, as shown in Figure 4d. While the cyclic voltammogram retains the characteristic features of a polycrystalline gold surface, subtle deviations appear when compared to the Au-only electrode. Most notably, the anodic peaks associated with gold oxidation, typically observed between approximately 1.3 and 1.65 V vs. RHE, appear broadened and less defined in the presence of the Nafion layer. Additionally, two minor peaks can be discerned at around 0.4 V vs. RHE in the anodic sweep and at around 0.3 V vs. RHE in the cathodic sweep. The QCM-D response closely mirrors the behavior previously observed for Nafion-coated platinum electrodes (Figure 4c). At potentials higher than 1.0 V vs. RHE, the mass changes correspond well to the oxidation and subsequent reduction of the gold surface. However, the total mass shift between oxidized and reduced states of the electrode is approximately 2.5 times larger than that observed for the uncoated Au-only electrode. At the same time, the dissipation remains largely constant within this potential region. But at lower potentials, specifically below 0.4 V vs. RHE, a pronounced dissipation peak emerges, reflecting a behavior similar to that of the platinum electrode presented in Figure 4c. This dissipation change coincides with a substantial increase in Sauerbrey mass. In the cathodic scan, this mass increase initiates at approximately 0.35 V vs. RHE, while in the anodic scan, the corresponding mass loss concludes around 0.45 V vs. RHE. These onset and endpoint

potentials align with the additional peaks identified in the voltammogram, suggesting a direct correlation between the electrochemical response and the observed mass and dissipation changes.

At first glance, the response of a Nafion film on a gold electrode appears similar to that observed on a platinum electrode in $HClO_4$. In both cases, the behavior differs significantly from that in H_2SO_4, as a pronounced increase in mass and dissipation is observed at low potentials. Importantly, in these cases, the response of the dissipation does not seem to be linked to oxidation or reduction processes occurring at the electrode surface. Changes in mass associated with faradaic processes, on the contrary, remain clearly identifiable and can be directly correlated with the oxidation and reduction peaks in the CV data. Overall, we interpret the simultaneous increases in mass and dissipation at low potential in a similar manner to previous observations, namely, as a consequence of changes in the viscoelastic properties of the Nafion film due to variations in water content and the resulting reorganization of the polymer structure. However, upon closer inspection, subtle differences emerge between the measurements on platinum and gold electrodes:

First, in the case of the gold electrode, the changes in mass and dissipation appear to coincide with additional, very weak faradaic processes. This suggests that adsorption/desorption of ionic groups may occur at low potentials, leading to a reorganization of the polymer structure. It is plausible that this involves the sulfonic acid end groups of the Nafion side chains, a behavior previously reported by Maduska et al. [39]. The absence of a similar signal on platinum electrodes is likely due to the overlap with the underpotential deposition of hydrogen atoms, which does not occur on gold surfaces.

Second, discrepancies in mass increase due to surface oxidation are observed between measurements with and without a Nafion film on gold electrodes, which cannot be seen with platinum electrodes. This is accompanied by changes in the CV data, suggesting that the process of gold oxidation in $HClO_4$ is influenced by the presence of a Nafion film. While the exact mechanisms are difficult to extract from the available data, it is reasonable to assume that the strong affinity of sulfonic acid groups for gold surfaces plays a key role in this behavior.

Taken together, these observations are consistent with the well-established understanding that anion adsorption significantly influences the properties of PGM-based catalysts [84, 85]. This highlights the importance of carefully considering electrolyte composition when evaluating PEMFC catalysts with ionomer, particularly to ensure comparability between measurements conducted in different electrolyte environments.

2.3 | EQCM-D Measurements of a PEMFC Electrode

The investigation of interactions between individual PEMFC electrode components has yielded valuable insights into how these materials respond to changes in electrode potential. To gain a more holistic understanding of the interplay between these processes under realistic conditions, we characterized a full PEMFC CL using EQCM-D. For this purpose, a quartz crystal with a carbon-coated top electrode was modified by spray-coating it with catalyst ink, followed by electrochemical characterization in 0.5 M H_2SO_4 at 25°C using CV at a scan rate of 50 mV s^{-1}.

Scanning electron microscopy (SEM) images of an electrode prepared in this manner are shown in Figure 5. Figure 5a shows a top view of the electrode, revealing minor variations in the density of the CL. However, the overall coverage appears sufficiently uniform. A cross-sectional view of the same electrode is shown in Figure 5b, where the individual layers are clearly distinguishable. At the bottom of the image, the quartz crystal is visible, coated by a bright-contrast gold layer. Above this lies the carbon layer, which appears darker in contrast followed by the PEMFC CL. The morphology of this layer is largely dictated by the highly porous carbon support structure. The average thickness of the CL was determined to be 1.52 µm, based on measurements at 25 arbitrarily selected locations, with a standard deviation of 0.43 µm.

The results of the EQCM-D measurements are shown in Figure 6. Figure 6a displays the outcome of the EQCM-D measurement during one cycle of the CV. The upper panel shows the voltammogram, which exhibits the characteristic features of polycrystalline platinum, including well-defined oxidation and reduction peaks. The lower panel presents the corresponding potential-dependent Sauerbrey mass and dissipation changes. The mass signal resembles that of a planar platinum electrode, with observable, though slightly attenuated, mass changes associated with the formation and reduction of platinum oxide at potentials

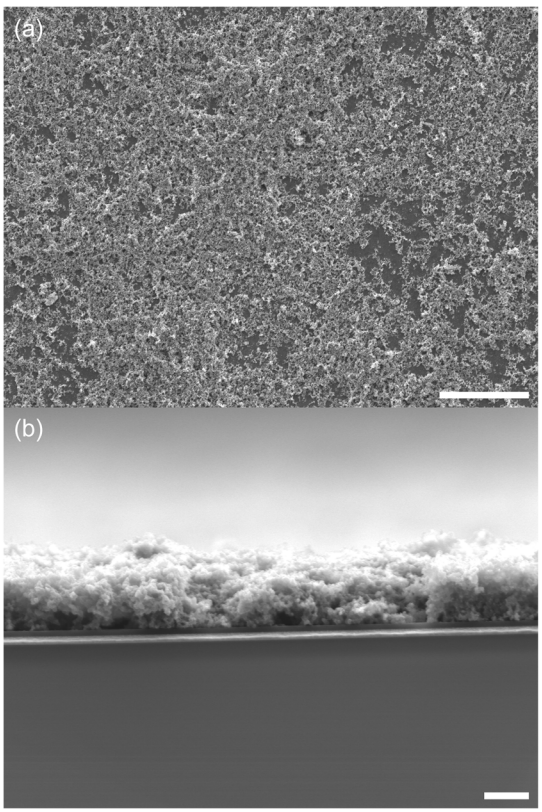

FIGURE 5 | (a) Top view SEM image of a Quartz crystal with a carbon top electrode spray-coated with PEMFC catalyst ink. The scale bar indicates 10 µm. (b) Cross section SEM image of the same Quartz crystal with a carbon top electrode spray-coated with PEMFC catalyst ink. The scale bar indicates 1 µm.

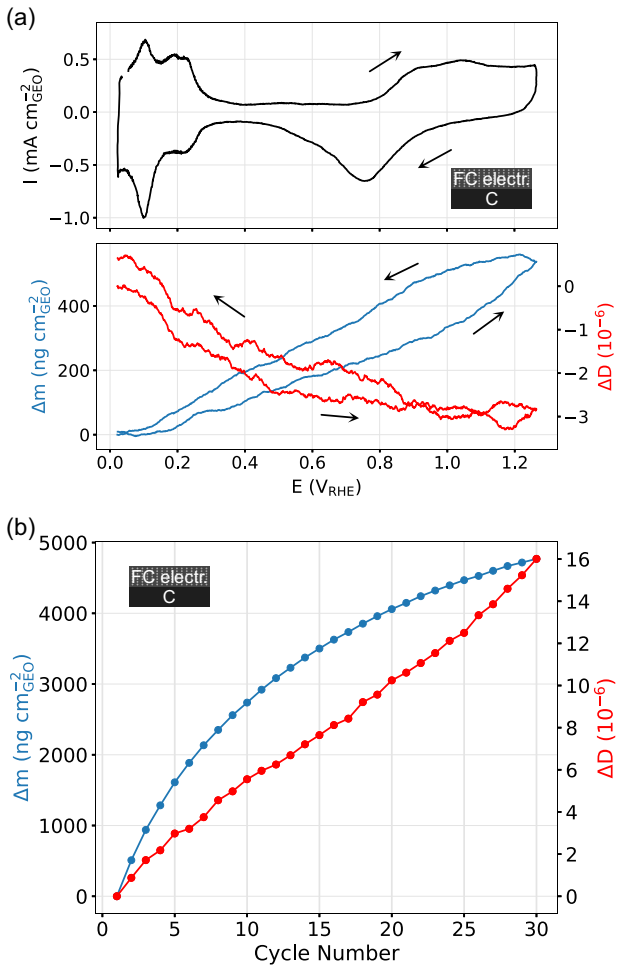

FIGURE 6 | (a) CV (black), Sauerbrey mass (blue), and dissipation (red) response during EQCM-D measurements of a carbon electrode spray-coated with PEMFC catalyst ink. (b) Sauerbrey mass (blue) and dissipation (red) change over 10 CV cycles during EQCM-D measurements of a carbon electrode spray-coated with PEMFC catalyst ink. All measurements were performed at 25°C in 0.5 M H_2SO_4 with a scan rate of 50 mV s^{-1}.

around 1.0 and 0.8 V vs. RHE, respectively. The hysteresis between the oxidation and reduction phases is clearly visible and reasonably matches the behavior observed in Figure 1d for a Pt/Nafion electrode. A comparable trend is also apparent in the dissipation response, which decreases during the forward scan toward more positive potential and increases again during the reverse scan, ultimately ending at a higher value than initially. Although fewer distinct features are discernible in the dissipation trace, the overall behavior remains consistent with that observed for the Nafion-coated platinum electrode.

This trend persists when examining the evolution of the Sauerbrey mass and dissipation over multiple CV cycles. As shown in Figure 6b, the Sauerbrey mass exhibits a pronounced increase during the initial cycles, followed by gradual saturation. Thus, it seems like the signal follows the general trend compared to the samples with planar geometry, but stabilization requires a larger total number of cycles. The dissipation increases steadily throughout the measurement window in a similar way as observed in Figure 3d. The absolute changes in mass and dissipation, however, differ significantly in magnitude, which can primarily be attributed to the fundamentally different morphology of the electrode compared to the planar structure of the Pt/Nafion electrodes. Generally, a quantitative analysis of the mass change of the entire CL is not possible in this case, as the thickness of the CL clearly exceeds the sensing depth of the QCM in aqueous solutions [86]. It is therefore reasonable to assume that the CL is not sensed uniformly by the QCM and that the numbers presented here cannot be directly compared to the results of the planar samples above. Nonetheless, the overall qualitative behavior of the CL during CV remains in agreement with the observations for the planar Pt/Nafion electrode. These results support the conclusion that the observed mass increase arises from amplified hydration of the Nafion phase embedded in the CL. As previously proposed for the planar electrode, this enhanced hydration is induced by the cyclic oxidation and reduction of the platinum surface, which appears to act as a pumping mechanism, drawing additional water into the polymer phase. However, due to the inherently porous structure of the CL, the mass transport and hydration processes are likely more spatially distributed and less well resolved in the QCM signal, therefore also requiring a higher number of potential cycles before reaching equilibrium. Taken together, these findings underscore the value of model electrode studies for isolating and understanding the individual contributions of specific PEMFC electrode components. The insights gained at the component level can subsequently be translated into more complex, realistic systems such as CLs, providing a clearer picture of the mechanisms at play in operational fuel cell environments.

3 | Conclusion

This study provides detailed insights into the potential-dependent interactions between Nafion ionomer and catalyst surfaces relevant to PEMFC electrodes. EQCM-D measurements of Nafion-coated platinum electrodes in 0.5 M H_2SO_4 reveal pronounced hydration dynamics of the ionomer film in response to electrochemical surface processes. Adsorption phenomena, as well as the oxidation and reduction of platinum, significantly influence the water content of the Nafion layer, in some cases irreversibly. Complementary measurements on carbon electrodes confirm that the observed ionomer response is governed by electrochemical surface reactions rather than the applied potential itself. Corresponding experiments on gold electrodes further support these findings, demonstrating pronounced but fully reversible changes in Nafion hydration associated with adsorption/desorption and redox processes and thereby suggesting a material-specific ionomer-electrode coupling. These modulations in water content induced by cyclic potential changes result, particularly on platinum, in a progressive and irreversible increase in Nafion hydration beyond its initial state. Substitution of the electrolyte with 0.1 M $HClO_4$ highlights the substantial role of anions in modulating these dynamics, with sulfate-containing media enhancing the ionomer response via stronger specific adsorption and interfacial restructuring. A comparison between EQCM-D measurements on planar, Nafion-coated platinum electrodes and an electrode spray-coated with a representative PEMFC CL reveals highly similar behavior, indicating that, based on the same mechanisms, amplified water absorption occurs in the ionomer during the CV. Hence, this study elucidates the nature of Nafion-catalyst interactions as a function

of electrode potential using EQCM-D, and demonstrates the value of simplified electrode architectures for probing fundamental interfacial phenomena. Our findings indicate that the structure and water content of the ionomer in a PEMFC electrode strongly depend on the oxidation state of the catalyst surface. Repeated variations in surface oxidation can induce a measurable increase in ionomer water content, already after a limited number of cycles. While this effect was observed over a relatively small number of cycles, its irreversible nature suggests that repeated cycling during start-up or activation could significantly alter ionomer properties, with potential implications for PEMFC performance. Importantly, such hydration changes may be beneficial during activation by improving proton conductivity and facilitating initial electrode wetting, although their long-term impact on durability remains to be clarified. Thereby, these insights contribute to a deeper mechanistic understanding of ionomer behavior under dynamic fuel cell operating conditions and offer meaningful context for optimizing activation protocols, which rely on changes in electrode hydration and structure induced by potential cycling.

4 | Experimental Section

4.1 | Quartz Crystal Preparations

The sample crystals were single-sided gold-coated quartz crystals custom ordered from Biolin Scientific with a fundamental frequency of 5 MHz. The backside was precoated with gold while the working electrode top side arrived uncoated and was then coated with gold, platinum, or carbon films via physical vapor deposition (PVD). The gold and platinum electrodes were coated with 200 nm thick layer of the respective metal as well as an adhesion layer of 3 nm titanium. The coating of the Au and Pt crystals was done in a Lesker PVD 225 by the Kurt J. Lesker Company. The carbon crystals were coated with a gold base layer (200 nm thickness), a carbon top layer (100 nm thickness), and titanium (3 nm thickness) adhesion layers underneath the gold layer and between the gold and carbon layer, whereby the carbon layer was added in an AVAC PVD HVC600 unit. The coated area was $0.227 \pm 0.003\ cm^2$, the sensitive area of the crystal is where the top electrode overlaps the bottom electrode, resulting in an active area of $0.197\ cm^2$.The crystals were cleaned before coating by progressive sonication in acetone (Sigma–Aldrich), isopropanol (VWR), and Milli-Q water (18 MΩ) for 10 min each. The crystals were then dried by nitrogen flow (N_2, grade N6.0, Strandmøllen). Additionally, the surface was pretreated by oxygen plasma at 100 W for 2 min in a Plasmatherm batchtop m/95 reactive ion etcher.

Following the fabrication of the electrodes, a Nafion coating was applied to the top side of some quartz crystals. For this purpose, a 5 wt% solution of Nafion 117 (Sigma–Aldrich) was diluted with isopropanol to a final concentration of 1 wt%. The resulting solution was uniformly distributed on the crystal surface via spin coating at 7000 rpm for a minimum of 2 min. After coating, the Nafion film was dried under ambient conditions. The thickness of the Nafion layer was determined using a Tencor Alpha Step 500 surface profiler, while its homogeneity was assessed by optical microscopy and AFM (Bruker Dimension ICON). Details of the evaluation are provided in the Supporting Information.

4.2 | PEMFC Catalyst Ink Preparation and Spray-Coating

PEMFC CLs were realized by applying a catalytic ink onto the QCM crystal using an automated spraying machine (SonoTech) in the laboratory of Applied Electrochemistry at KTH. The preparation of the ink consisted of adding a solution of Milli-Q water and isopropanol (Sigma–Aldrich) with a 1:1 wt. ratio to the Pt/C powder (40% Pt on Vulcan C, Fuel Cell Store) while stirring. Once uniformly dispersed, the ionomer solution (Nafion in 5 wt.% solution, Aldrich) was added dropwise to the ink while still stirring. The final ink was composed of 1 wt.% solid content over the entire solution, of which the I/C ratio was 0.3.

The ink was then sonicated in an ice bath for an hour and mounted onto the machine. To achieve a homogeneous coverage while still maintaining a reasonable electrode thickness, two layers of ink were deposited on the support one after the other, while the hotplate holder was set to 80°C to ensure an adequate solvent evaporation rate.

4.3 | EQCM-D Measurements

Prior to each measurement, the quartz crystals were thoroughly rinsed with Milli-Q water (18.2 MΩ cm), dried under a nitrogen stream (N_2, grade N6.0, Strandmøllen), and subsequently mounted into a dip holder from MicroVacuum. The dip holder, made of polyether ether ketone (PEEK), was sealed using O-rings from fluorinated fluoropolymer elastomer (FFPM) by evenly tightening nylon screws after carefully positioning the crystal. Electrolyte solutions of 0.5 M H_2SO_4 and 0.1 M $HClO_4$ were prepared using concentrated suprapure H_2SO_4 and $HClO_4$ (Merck KGaA) diluted with Milli-Q water. All electrochemical measurements were conducted in a three-electrode configuration, with continuous argon (Ar, grade N6.0, Strandmøllen) purging of the electrolyte solution at standard temperature (298.15 K). The quartz crystal mounted in the dip holder served as the working electrode. A Hg/Hg_2SO_4 reference electrode (B-3610+, SI Analytics) was used for all measurements. The potential of the reference electrode relative to the RHE was verified before each experiment using a platinum wire in a H_2-saturated electrolyte. All potentials reported in this study were converted to the RHE scale. A SPK-grade graphite rod (6.15 mm diameter, Thermo Scientific Chemicals) was employed as the counter electrode. CV measurements were performed using a SP-300 potentiostat (Biologic), controlled via EC-Lab software (Biologic). Simultaneously, the dip holder was connected to a QSense Explorer frequency analyzer (Biolin Scientific) via a custom-built adapter, enabling acquisition of data from the QCM-D using QSoft401 software (Biolin Scientific).

At the beginning of each experiment, electrodes made of platinum, carbon, gold, and catalyst ink were subjected to electrochemical conditioning. This was performed by cycling the potential between 0.05 V vs. RHE and the respective UPL. The scan rate during this conditioning CV was $100\ mV\ s^{-1}$, applied for a minimum of 10 and up to 50 cycles. This procedure served to enhance the characteristic features in the voltammograms and facilitated the acquisition of CV representative of the respective polycrystalline metal surfaces. Subsequently, the actual measurements were conducted as CVs over 10 cycles at a scan rate of $50\ mV\ s^{-1}$ within a potential window of 0.05 V vs. RHE to the corresponding UPL. For platinum, carbon, and catalyst ink

electrodes, the UPL was set to 1.25 V vs. RHE, while for gold electrodes it was 1.8 V vs. RHE. The lower potential limit was chosen to ensure complete hydrogen underpotential deposition on platinum electrodes without inducing hydrogen evolution. The UPL was adjusted to allow observation of oxide formation on platinum and gold electrodes, respectively.

Simultaneous QCM-D measurements were performed by tracking changes in the resonance frequency of the quartz crystal relative to the initial frequency using the frequency analyzer. At least three overtones were monitored during each experiment. For each overtone, the change in dissipation, representing the energy loss due to damping, was also recorded for the respective resonance oscillation. This dissipation tracking was likewise performed using the Qsense Explorer, which determines dissipation based on the decay time of an induced oscillation after removal of the driving force. Mass changes were calculated from the frequency shifts using the Sauerbrey equation [40].

$$\Delta m = -\Delta f_n \frac{\sqrt{\rho_q \mu_q}}{2nf_0^2} \quad (5)$$

where Δm is the mass change, Δf_n is the frequency shift of the n-th overtone, ρ_q is the density, and μ_q is the shear modulus of an AT-cut quartz crystal, and f_0 stands for the initial resonant frequency. An average mass change was derived from the individual overtones. To minimize systematic errors, electrochemical measurements were initiated only after the frequency drift stabilized to less than 1 Hz over 5 min, corresponding to a mass drift of approximately 0.06 ng s^{-1}, which is negligible compared to the mass changes of interest. Synchronization of the electrochemical and frequency signals was achieved via a trigger signal sent from the QSoft401 software to the potentiostat, which initiated the electrochemical measurement upon detection.

All glassware and laboratory equipment used in the experiments were cleaned, where possible, by soaking in freshly prepared piranha solution (4:1 concentrated sulfuric acid to 30% hydrogen peroxide) for at least 3 h, followed by thorough rinsing with Milli-Q water. More delicate components, such as the dip holder and O-rings, were cleaned by rinsing with isopropanol and Milli-Q water.

Acknowledgments

This project was financially supported by the Swedish Foundation for Strategic Research (project no. ARC19−0026) and performed within the Competence Centre for Catalysis, which is hosted by the Chalmers University of Technology and financially supported by the Swedish Energy Agency (project no. 52689−1) and the member companies Johnson Matthey, Perstorp, PowerCell, Preem, Scania CV, Umicore, and Volvo Group. The authors acknowledge the use of the Chalmers Material Analysis Laboratory, CMAL, and the use of the Nanofabrication Laboratory at Chalmers University of Technology. The researchers at KTH acknowledge the governmental initiative StandUp for Energy and Swedish Energy Agency through Swedish Electromobility Centre for financial support.

Funding

Stiftelsen för Strategisk Forskning (ARC19-0026); Energimyndigheten (52689−1).

Conflicts of Interest

The authors declare no conflicts of interest.

Data Availability Statement

The data that support the findings of this study are available from the corresponding author upon reasonable request.

References

1. J. O. Abe, A. P. I. Popoola, E. Ajenifuja, and O. M. Popoola, "Hydrogen Energy, Economy and Storage: Review and Recommendation," *International Journal of Hydrogen Energy* 44 (2019): 15072–15086.

2. I. Staffell, D. Scamman, A. V. Abad, et al., "The Role of Hydrogen and Fuel Cells in the Global Energy System," *Energy & Environmental Science* 12 (2019): 463–491.

3. H. A. Gasteiger, J. E. Panels, and S. G. Yan, "Dependence of PEM Fuel Cell Performance on Catalyst Loading," *Journal of Power Sources* 127 (2004): 162–171.

4. E. Antolini, "Structural Parameters of Supported Fuel Cell Catalysts: The Effect of Particle Size, Inter-Particle Distance and Metal Loading on Catalytic Activity and Fuel Cell Performance," *Applied Catalysis B: Environment and Energy* 181 (2016): 298–313.

5. A. Katsaounis, S. P. Balomenou, D. Tsiplakides, M. Tsampas, and C. G. Vayenas, "The Role of Potential-Dependent Electrolyte Resistance in the Performance, Steady-State Multiplicities and Oscillations of PEM Fuel Cells: Experimental Investigation and Macroscopic Modelling," *Electrochimica Acta* 50 (2005): 5132–5143.

6. A. Kongkanand and M. F. Mathias, "The Priority and Challenge of High-Power Performance of Low-Platinum Proton-Exchange Membrane Fuel Cells," *Journal of Physical Chemistry Letters* 7 (2016): 1127–1137.

7. A. Ohma, K. Fushinobu, and K. Okazaki, "Influence of Nafion Film on Oxygen Reduction Reaction and Hydrogen Peroxide Formation on Pt Electrode for Proton Exchange Membrane Fuel Cell," *Electrochimica Acta* 55 (2010): 8829–8838.

8. P. Toudret, A. Chenneviere, J.-F. Blachot, et al., "Evidence of Well-Dispersed Ionomer in the Cathode Catalyst Layer of Proton Exchange Membrane Fuel Cell by Small Angle Scattering, and Effect of Its Content on Performance," *Journal of the Electrochemical Society* 172 (2025): 034515.

9. M. Arun, S. Giddey, P. Joseph, and D. S. Dhawale, "Challenges and Mitigation Strategies for General Failure and Degradation in Polymer Electrolyte Membrane-Based Fuel Cells and Electrolysers," *Journal of Materials Chemistry A* 13 (2025): 11236–11263.

10. F. Van Der Linden, E. Pahon, S. Morando, and D. Bouquain, "A Review on the Proton-Exchange Membrane Fuel Cell Break-in Physical Principles, Activation Procedures, and Characterization Methods," *Journal of Power Sources* 575 (2023): 233168.

11. D. A. Cullen, K. C. Neyerlin, R. K. Ahluwalia, et al., "New Roads and Challenges for Fuel Cells in Heavy-Duty Transportation," *Nature Energy* 6 (2021): 462–474.

12. V. Shokhen, L. Strandberg, M. Skoglundh, and B. Wickman, "Fuel Cell Electrode Degradation Followed by Identical Location Transmission Electron Microscopy," *Journal of Materials Chemistry A* 11 (2023): 21029–21035.

13. L. M. Roen, C. H. Paik, and T. D. Jarvi, "Electrocatalytic Corrosion of Carbon Support in PEMFC Cathodes," *Electrochemical and Solid-State Letters* 7 (2003): A19.

14. S. C. Ball, S. L. Hudson, D. Thompsett, and B. Theobald, "An Investigation into Factors Affecting the Stability of Carbons and Carbon Supported Platinum and Platinum/Cobalt Alloy Catalysts during

1.2 V Potentiostatic Hold Regimes at a Range of Temperatures," *Journal of Power Sources* 171 (2007): 18–25.

15. K. H. Kangasniemi, D. A. Condit, and T. D. Jarvi, "Characterization of Vulcan Electrochemically Oxidized Under Simulated PEM Fuel Cell Conditions," *Journal of the Electrochemical Society* 151 (2004): E125.

16. Z. Y. Liu, J. L. Zhang, P. T. Yu, et al., "Transmission Electron Microscopy Observation of Corrosion Behaviors of Platinized Carbon Blacks Under Thermal and Electrochemical Conditions," *Journal of the Electrochemical Society* 157 (2010): B906.

17. B. Vion-Dury, M. Chatenet, L. Guétaz, and F. Maillard, "Determination of Aging Markers and Their Use as a Tool to Characterize Pt/C Nanoparticles Degradation Mechanism in Model PEMFC Cathode Environment," *ECS Transactions* 41 (2011): 697.

18. P. S. Ruvinskiy, A. Bonnefont, C. Pham-Huu, and E. R. Savinova, "Using Ordered Carbon Nanomaterials for Shedding Light on the Mechanism of the Cathodic Oxygen Reduction Reaction," *Langmuir : the Acs Journal of Surfaces and Colloids* 27 (2011): 9018–9027.

19. K. Ono, Y. Yasuda, K. Sekizawa, N. Takeuchi, T. Yoshida, and M. Sudoh, "Evaluation of Pt/C Catalyst Degradation and H2O2 Formation Changes Under Simulated PEM Fuel Cell Condition by a Rotating ring-Disk Electrode," *Electrochimica Acta* 97 (2013): 58–65.

20. D. Kurniawan, H. Arai, S. Morita, and K. Kitagawa, "Chemical Degradation of Nafion Ionomer at a Catalyst Interface of Polymer Electrolyte Fuel Cell by Hydrogen and Oxygen Feeding in the Anode," *Microchemical Journal* 106 (2013): 384–388.

21. T. Okada in Handb, *Fuel Cells* (John Wiley & Sons, Ltd., 2010).

22. M. Zatoń, J. Rozière, and D. J. Jones, "Current Understanding of Chemical Degradation Mechanisms of Perfluorosulfonic Acid Membranes and Their Mitigation Strategies: A Review," *Sustainable Energy & Fuels* 1 (2017): 409–438.

23. Y. Li, D. A. Dillard, Y.-H. Lai, et al., "Experimental Measurement of Stress and Strain in Nafion Membrane during Hydration Cycles," *Journal of the Electrochemical Society* 159 (2011): B173.

24. H. Li, Y. Tang, Z. Wang, et al., "A Review of Water Flooding Issues in the Proton Exchange Membrane Fuel Cell," *Journal of Power Sources* 178 (2008): 103–117.

25. Q. He, N. S. Suraweera, D. C. Joy, and D. J. Keffer, "Structure of the Ionomer Film in Catalyst Layers of Proton Exchange Membrane Fuel Cells," *Journal of Physical Chemistry C* 117 (2013): 25305–25316.

26. A. Nouri-Khorasani, K. Malek, A. Malek, T. Mashio, D. P. Wilkinson, and M. H. Eikerling, "Molecular Modeling of the Proton Density Distribution in a Water-Filled Slab-Like Nanopore Bounded by Pt Oxide and Ionomer," *Catalysis Today* 262 (2016): 133–140.

27. V. M. Fernández-Alvarez, K. Malek, M. H. Eikerling, A. Young, M. Dutta, and E. Kjeang, "Molecular Dynamics Study of Reaction Conditions at Active Catalyst-Ionomer Interfaces in Polymer Electrolyte Fuel Cells," *Journal of the Electrochemical Society* 169 (2022): 024506.

28. L. Guetaz, M. Lopez-Haro, S. Escribano, et al., "Catalyst-Layer Ionomer Imaging of Fuel Cells," *ECS Transactions* 69 (2015): 455.

29. L. G. A. Melo, A. P. Hitchcock, J. Jankovic, J. Stumper, D. Susac, and V. Berejnov, "Quantitative Mapping of Ionomer in Catalyst Layers by Electron and X-Ray Spectromicroscopy," *ECS Transactions* 80 (2017): 275.

30. T. Morawietz, M. Handl, C. Oldani, K. A. Friedrich, and R. Hiesgen, "Quantitative In Situ Analysis of Ionomer Structure in Fuel Cell Catalytic Layers," *ACS Applied Materials & Interfaces* 8 (2016): 27044–27054.

31. M. Rodahl, F. Höök, C. Fredriksson, et al., "Simultaneous Frequency and Dissipation Factor QCM Measurements of Biomolecular Adsorption and Cell Adhesion," *Faraday Discussions* 107 (1997): 229–246.

32. D. Johannsmann, K. Mathauer, G. Wegner, and W. Knoll, "Viscoelastic Properties of Thin Films Probed with a Quartz-Crystal Resonator," *Physical Review B* 46 (1992): 7808–7815.

33. F. Gloaguen, J.-M. Léger, and C. Lamy, "An Electrochemical Quartz Crystal Microbalance Study of the Hydrogen Underpotential Deposition at a Pt Electrode," *Journal of Electroanalytical Chemistry* 467 (1999): 186–192.

34. K. Shimazu and H. Kita, "In Situ Measurements of Water Adsorption on a Platinum Electrode by an Electrochemical Quartz Crystal Microbalance," *Journal of Electroanalytical Chemistry* 341 (1992): 361–367.

35. L. Strandberg, V. Shokhen, M. Luneau, G. Lindbergh, C. Lagergren, and B. Wickman, *"Comparison of Oxygen Adsorption and Platinum Dissolution in Acid and Alkaline Solutions Using Electrochemical Quartz Crystal Microbalance" ChemElectroChem*, 9 (2022):e202200591.

36. G. Jerkiewicz, G. Vatankhah, J. Lessard, M. P. Soriaga, and Y.-S. Park, "Surface-Oxide Growth at Platinum Electrodes in Aqueous H2SO4," *Electrochimica Acta* 49 (2004): 1451–1459.

37. L. Strandberg, V. Shokhen, M. Skoglundh, and B. Wickman, "Carbon Support Corrosion in PEMFCs Followed by Identical Location Electron Microscopy," *ACS Catalysis* 14 (2024): 8494–8504.

38. T. Masuda, F. Sonsudin, P. R. Singh, H. Naohara, and K. Uosaki, "Potential-Dependent Adsorption and Desorption of Perfluorosulfonated Ionomer on a Platinum Electrode Surface Probed by Electrochemical Quartz Crystal Microbalance and Atomic Force Microscopy," *Journal of Physical Chemistry C* 117 (2013): 15704–15709.

39. T. Masuda, K. Ikeda, and K. Uosaki, "Potential-Dependent Adsorption/Desorption Behavior of Perfluorosulfonated Ionomer on a Gold Electrode Surface Studied by Cyclic Voltammetry, Electrochemical Quartz Microbalance, and Electrochemical Atomic Force Microscopy," *Langmuir : the Acs Journal of Surfaces and Colloids* 29 (2013): 2420–2426.

40. J. Kankare, "Sauerbrey Equation of Quartz Crystal Microbalance in Liquid Medium," *Langmuir : the Acs Journal of Surfaces and Colloids* 18 (2002): 7092–7094.

41. W. Visscher, J. F. E. Gootzen, A. P. Cox, and J. A. R. van Veen, "Electrochemical Quartz Crystal Microbalance Measurements of CO Adsorption and Oxidation on Pt in Various Electrolytes," *Electrochimica Acta* 43 (1998): 533–547.

42. V. I. Birss, M. Chang, and J. Segal, "Platinum Oxide Film Formation—reduction: An in-Situ Mass Measurement Study," *Journal of Electroanalytical Chemistry* 355 (1993): 181–191.

43. M. Osawa, M. Tsushima, H. Mogami, G. Samjeské, and A. Yamakata, "Structure of Water at the Electrified Platinum–Water Interface: A Study by Surface-Enhanced Infrared Absorption Spectroscopy," *Journal of Physical Chemistry C* 112 (2008): 4248–4256.

44. A. A. Topalov, I. Katsounaros, M. Auinger, et al., "Dissolution of Platinum: Limits for the Deployment of Electrochemical Energy Conversion?," *Angewandte Chemie International Edition* 51 (2012): 12613–12615.

45. R. Lucklum, C. Behling, and P. Hauptmann, "Role of Mass Accumulation and Viscoelastic Film Properties for the Response of Acoustic-Wave-Based Chemical Sensors," *Analytical Chemistry* 71 (1999): 2488–2496.

46. B. Wickman, H. Grönbeck, P. Hanarp, and B. Kasemo, "Corrosion Induced Degradation of Pt/C Model Electrodes Measured with Electrochemical Quartz Crystal Microbalance," *Journal of the Electrochemical Society* 157 (2010): B592.

47. C. Shengli, W. Bingliang, and Z. Hong, "An EQCM Study of the Electrochemical Behaviors of Polycrystalline Gold Electrode in Sulfuric Acid Solution," *Wuhan University Journal of Natural Sciences* 3 (1998): 102–107.

48. V. Tsionsky, L. Daikhin, and E. Gileadi, "Response of the Electrochemical Quartz Crystal Microbalance for Gold Electrodes in

the Double-Layer Region," *Journal of the Electrochemical Society* 143 (1996): 2240.

49. S. Jiang, Q. Xiang, Z. Xie, et al., "Influence of the Pt/Ionomer/Water Interface on the Oxygen Reduction Reaction: Insights into the Micro-Three-Phase Interface," *Chemical Science* 15 (2024): 19290–19298.

50. I. Ledezma-Yanez, W. D. Z. Wallace, P. Sebastián-Pascual, V. Climent, J. M. Feliu, and M. T. M. Koper, "Interfacial Water Reorganization as a pH-Dependent Descriptor of the Hydrogen Evolution Rate on Platinum Electrodes," *Nature Energy* 2 (2017): 1–7.

51. P. Li, Y. Jiang, Y. Hu, et al., "Hydrogen Bond Network Connectivity in the Electric Double Layer Dominates the Kinetic pH Effect in Hydrogen Electrocatalysis on Pt," *Nature Catalysis* 5 (2022): 900–911.

52. R. Schumacher, G. Borges, and K. K. Kanazawa, "The Quartz Microbalance: A Sensitive Tool to Probe Surface Reconstructions on Gold Electrodes in Liquid," *Surface Science Letters* 163 (1985): L621–L626.

53. S. Bruckenstein and M. Shay, "An In Situ Weighing Study of the Mechanism for the Formation of the Adsorbed Oxygen Monolayer at a Gold Electrode," *Journal of Electroanalytical Chemistry and Interfacial Electrochemistry* 188 (1985): 131–136.

54. F. G. Donnan, "Theorie der Membrangleichgewichte Und Membranpotentiale Bei Vorhandensein Von Nicht Dialysierenden Elektrolyten. Ein Beitrag Zur Physikalisch-Chemischen Physiologie," *Zeitschrift für Elektrochemie Und Angewandte Physikalische Chemie* 17 (1911): 572–581.

55. H. Strathmann, A. Grabowski, and G. Eigenberger, "Ion-Exchange Membranes in the Chemical Process Industry," *Industrial & Engineering Chemistry Research* 52 (2013): 10364–10379.

56. N. Kimura, H. Matsumoto, Y. Konosu, R. Yamamoto, M. Minagawa, and A. Tanioka, "Membrane Potential across Anion-Exchange Membranes in Acidic Solution System," *Journal of Colloid and Interface Science* 286 (2005): 288–293.

57. G. Zhang and C. Wu, "Quartz Crystal Microbalance Studies on Conformational Change of Polymer Chains at Interface," *Macromolecular Rapid Communications* 30 (2009): 328–335.

58. H. L. Bandey, A. R. Hillman, M. J. Brown, and S. J. Martin, "Viscoelastic Characterization of Electroactive Polymer Films at the Electrode/Solution Interface," *Faraday Discussions* 107 (1997): 105–121.

59. F. Höök, B. Kasemo, T. Nylander, C. Fant, K. Sott, and H. Elwing, "Variations in Coupled Water, Viscoelastic Properties, and Film Thickness of a Mefp-1 Protein Film during Adsorption and Cross-Linking: A Quartz Crystal Microbalance with Dissipation Monitoring, Ellipsometry, and Surface Plasmon Resonance Study," *Analytical Chemistry* 73 (2001): 5796–5804.

60. M. Chen, J. Ma, Z. Wang, X. Zhang, and Z. Wu, "Insights into Iron Induced Fouling of Ion-Exchange Membranes Revealed by a Quartz Crystal Microbalance with Dissipation Monitoring," *RSC Advances* 7 (2017): 36555–36561.

61. Y.-F. Huang, P. J. Kooyman, and M. T. M. Koper, "Intermediate Stages of Electrochemical Oxidation of Single-Crystalline Platinum Revealed by In Situ Raman Spectroscopy," *Nature Communications* 7 (2016): 12440.

62. M. Ekimova, C. Kleine, J. Ludwig, et al., "From Local Covalent Bonding to Extended Electric Field Interactions in Proton Hydration," *Angewandte Chemie International Edition* 61 (2022): e202211066.

63. Q. Zhao, P. Majsztrik, and J. Benziger, "Diffusion and Interfacial Transport of Water in Nafion," *Journal of Physical Chemistry B* 115 (2011): 2717–2727.

64. P. A. Thiel and T. E. Madey, "The Interaction of Water with Solid Surfaces: Fundamental Aspects," *Surface Science Reports* 7 (1987): 211–385.

65. O. M. Magnussen, J. Hageböck, J. Hotlos, and R. J. Behm, "In Situ Scanning Tunnelling Microscopy Observations of a Disorder–order Phase Transition in Hydrogensulfate Adlayers on Au(111)," *Faraday Discussions* 94 (1992): 329–338.

66. K. Ataka, M. Osawa, "In Situ Infrared Study of Water–Sulfate Coadsorption on Gold(111) in Sulfuric Acid Solutions," *Langmuir* 14 (1998): 951–959.

67. T. Frelink, W. Visscher, and J. A. R. van Veen, "Measurement of the Ru Surface Content of Electrocodeposited PtRu Electrodes with the Electrochemical Quartz Crystal Microbalance: Implications for Methanol and CO Electrooxidation," *Langmuir : the Acs Journal of Surfaces and Colloids* 12 (1996): 3702–3708.

68. M. Watanabe, H. Uchida, and N. Ikeda, "Electrochemical Quartz Crystal Microbalance Study of Copper Ad-Atoms on Gold and Platinum Electrodes Part I. Adsorption of Anions in Sulfuric Acid," *Journal of Electroanalytical Chemistry* 380 (1995): 255–260.

69. Z. Jusys and S. Bruckenstein, "Electrochemical Quartz Crystal Microgravimetry of Gold in Perchloric and Sulfuric Acid Solutions," *Electrochemical and Solid-State Letters* 1 (1998): 74.

70. S. Cherevko, A. A. Topalov, A. R. Zeradjanin, I. Katsounaros, and K. J. J. Mayrhofer, "Gold Dissolution: Towards Understanding of Noble Metal Corrosion," *RSC Advances* 3 (2013): 16516–16527.

71. M. Smiljanić, U. Petek, M. Bele, et al., "Electrochemical Stability and Degradation Mechanisms of Commercial Carbon-Supported Gold Nanoparticles in Acidic Media," *Journal of Physical Chemistry C* 125 (2021): 635–647.

72. Z. Ghelichkhah, R. Srinivasan, D. D. Macdonald, and G. S. Ferguson, "Anion-Catalyzed Active Dissolution Model for the Electrochemical Adsorption of Bisulfate, Sulfate, and Oxygen on Gold in H2SO4 Solution," *Electrochimica Acta* 439 (2023): 141515.

73. C. Iojoiu, E. Guilminot, F. Maillard, et al., "Membrane and Active Layer Degradation Following PEMFC Steady-State Operation: II. Influence of on Membrane Properties," *Journal of the Electrochemical Society* 154 (2007): B1115.

74. S. Ueda, S. Koizumi, and Y. Tsutsumi, "Initial Conditioning of a Polymer Electrolyte Fuel Cells: The Relationship between Microstructure Development and Cell Performance, Investigated by Small-Angle Neutron Scattering," *Results in Physics* 12 (2019): 1871–1879.

75. A. Kusoglu and A. Z. Weber in, *Polym. Energy Storage Deliv. Polyelectrolytes Batter. Fuel Cells* (American Chemical Society, 2012), 175–199.

76. J. Li, X. Yang, H. Tang, and M. Pan, "Durable and High Performance Nafion Membrane Prepared through High-Temperature Annealing Methodology," *Journal of Membrane Science* 361 (2010): 38–42.

77. G. Alberti, R. Narducci, and M. Sganappa, "Effects of Hydrothermal/Thermal Treatments on the Water-Uptake of Nafion Membranes and Relations with Changes of Conformation, Counter-Elastic Force and Tensile Modulus of the Matrix," *Journal of Power Sources* 178 (2008): 575–583.

78. R. Narducci, P. Knauth, J.-F. Chailan, and M. L. D. Vona, "How to Improve Nafion with Tailor Made Annealing," *RSC Advances* 8 (2018): 27268–27274.

79. K. Berkesi, D. Horváth, Z. Németh, K. Varga, L. Péter, and T. Pintér, "Comparative Study of the Adsorption of SO42-/HSO4- and Cl– Anions on Smooth and rough Surfaces of Noble Metal Electrodes by In Situ Radiotracer Thin Gap Method," *Journal of Electroanalytical Chemistry* 712 (2014): 151–160.

80. J. C. Hey, L. C. Smeeton, M. T. Oakley, and R. L. Johnston, "Isomers and Energy Landscapes of Perchlorate–Water Clusters and a Comparison to Pure Water and Sulfate–Water Clusters," *Journal of Physical Chemistry A* 120 (2016): 4008–4015.

81. J. T. Kelly, M. Mayer, A. C. Kennedy, C. Schemel, and K. R. Asmis, "Probing the Propensity of Perchlorate Anions for Surface Solvation by

Infrared Photodissociation Spectroscopy," *Journal of Chemical Physics* 148 (2018): 222840.

82. V. Vchirawongkwin, B. M. Rode, and I. Persson, "Structure and Dynamics of Sulfate Ion in Aqueous Solution--an Ab Initio QMCF MD Simulation and Large Angle X-Ray Scattering Study," *Journal of Physical Chemistry B* 111 (2007): 4150–4155.

83. G. A. Attard, A. Brew, K. Hunter, J. Sharman, and E. Wright, "Specific Adsorption of Perchlorate Anions on Pt{hkl} Single Crystal Electrodes," *Physical Chemistry Chemical Physics* 16 (2014): 13689–13698.

84. V. Stamenkovic, N. M. Markovic, and P. N. Ross, "Structure-Relationships in Electrocatalysis: Oxygen Reduction and Hydrogen Oxidation Reactions on Pt(111) and Pt(100) in Solutions Containing Chloride Ions," *Journal of Electroanalytical Chemistry* 500 (2001): 44–51.

85. M. D. Maciá, J. M. Campiña, E. Herrero, and J. M. Feliu, "On the Kinetics of Oxygen Reduction on Platinum Stepped Surfaces in Acidic Media," *Journal of Electroanalytical Chemistry* 564 (2004): 141–150.

86. K. Keiji Kanazawa and J. G. Gordon, "The Oscillation Frequency of a Quartz Resonator in Contact with Liquid," *Analytica Chimica Acta* 175 (1985): 99–105.

Supporting Information

Additional supporting information can be found online in the Supporting Information section. **Supporting Fig. S1:** Optical (a, b) and AFM (c, d) images of Pt electrodes on quartz crystals used for EQCM-D measurements, both without (a, c) and with (b, d) a 30 nm Nafion layer. **Supporting Fig. S2:** Comparison of CV (black), Sauerbrey mass (blue) and dissipation (red) response during EQCM-D measurements of platinum, carbon and gold electrodes with and without an approximately 30 nm thin layer of Nafion. The measurements were performed at 25°C in 0.5 M H_2SO_4 with a scan rate of 50 mV s^{-1}. Here, the respective case with and without Nafion layer are shown in the same plot. a) presents the data for platinum electrodes, b) presents the data for carbon electrodes and c) presents the data for gold electrodes. **Supporting Fig. S3:** Comparison of CV (black), Sauerbrey mass (blue) and dissipation (red) response over 10 consecutive CV cycles during EQCM-D measurements of platinum electrodes a) without and b) with an approximately 30 nm thin layer of Nafion. The measurements were performed at 25°C in 0.5 M H_2SO_4 with a scan rate of 50 mV s^{-1}. **Supporting Fig. S4:** Comparison of CV (black), Sauerbrey mass (blue) and dissipation (red) response during EQCM-D measurements of gold electrodes a) without and b) with an approximately 30 nm thin layer of Nafion. The measurements were performed at 25°C in 0.5 M H_2SO_4 with a scan rate of 50 mV s^{-1} in the potential range of 0.05 V to 1.4 V or 1.3 V, respectively. **Supporting Fig. S5:** Comparison of CV (black), Sauerbrey mass (blue) and dissipation (red) response during EQCM-D measurements of platinum and gold electrodes with and without an approximately 30 nm thin layer of Nafion. The measurements were performed at 25°C in 0.1 M $HClO_4$ with a scan rate of 50 mV s^{-1}. Here, the respective case with and without Nafion layer are shown in the same plot. a) presents the data for platinum electrodes and b) presents the data for gold electrodes. **Supporting Table S1**: Thickness of a Nafion coating on a quartz crystal for QCM as a function of Nafion solution concentration, measured using a Tencor Alpha Step 500 surface profiler.